

**Central Arctic
atmospheric summer
conditions during
ASCOS**

M. Tjernström et al.

[Title Page](#)[Abstract](#)[Introduction](#)[Conclusions](#)[References](#)[Tables](#)[Figures](#)[Back](#)[Close](#)[Full Screen / Esc](#)[Printer-friendly Version](#)[Interactive Discussion](#)

⁷ Max Planck Institute for Meteorology, Hamburg, Germany

⁸ Finnish Meteorological Institute, Helsinki, Finland

⁹ Rosenstiel School of Marine and Atmospheric Sciences, University of Miami, Miami, FL, USA

Received: 19 December 2011 – Accepted: 21 January 2012 – Published: 3 February 2012

Correspondence to: M. Tjernström (michaelt@misu.su.se)

Published by Copernicus Publications on behalf of the European Geosciences Union.

Abstract

Understanding the rapidly changing climate in the Arctic is limited by a lack of understanding of underlying strong feedback mechanisms that are specific to the Arctic. Progress in this field can only be obtained by process-level observations; this is the motivation for intensive ice-breaker-based campaigns such as that described in this paper: the Arctic Summer Cloud-Ocean Study (ASCOS). However, detailed field observations also have to be put in the context of the larger-scale meteorology, and short field campaigns have to be analysed within the context of the underlying climate state and temporal anomalies from this.

To aid in the analysis of other parameters or processes observed during this campaign, this paper provides an overview of the synoptic-scale meteorology and its climatic anomaly during the ASCOS field deployment. It also provides a statistical analysis of key features during the campaign, such as some key meteorological variables, the vertical structure of the lower troposphere and clouds, and energy fluxes at the surface. In order to assess the representativity of the ASCOS results, we also compare these features to similar observations obtained during three earlier summer experiments in the Arctic Ocean, the AOE-96, SHEBA and AOE-2001 expeditions.

We find that these expeditions share many key features of the summertime lower troposphere. Taking ASCOS and the previous expeditions together, a common picture emerges with a large amount of low-level cloud in a well-mixed shallow boundary layer, capped by a weak to moderately strong inversion where moisture, and sometimes also cloud top, penetrate into the lower parts of the inversion. Much of the boundary-layer mixing is due to cloud-top cooling and subsequent buoyant overturning of the cloud. The cloud layer may, or may not, be connected with surface processes depending on the depths of the cloud and surface-based boundary layers and on the relative strengths of surface-shear and cloud-buoyancy turbulence generation. The latter also implies a connection between the cloud layer and the free troposphere through entrainment at cloud top.

Central Arctic atmospheric summer conditions during ASCOS

M. Tjernström et al.

Title Page

Abstract

Introduction

Conclusions

References

Tables

Figures



Back

Close

Full Screen / Esc

Printer-friendly Version

Interactive Discussion



1 Introduction

The rapidly changing Arctic climate over the last few decades (IPCC, 2007; ACIA, 2005; Richter-Menge, 2011) has focused significant scientific attention on this region. Arctic near-surface temperatures are currently rising at a rate more than twice that of the global average (e.g. Richter-Menge, 2011) and Arctic sea-ice is declining in all seasons, but most dramatically in summer (e.g., Lindsay and Zhang, 2005; Serreze et al., 2007; Overland, 2009). Many other aspects also show an “Arctic amplification” (Serreze and Francis, 2006). Although no consensus exists about primary reasons for the Arctic amplification, it is likely related to powerful feedbacks in the Arctic climate system, some of which are related to clouds and surface albedo.

Climate modeling is an indispensable tool in understanding the complex climate system; however, state-of-the-art global climate models have significant problems with the Arctic (Walsh et al., 2002; Chapman and Walsh, 2007). For example, the inter-model spread in climate projections for the end of this century in the Intergovernmental Panel on Climate Change Fourth Assessment Report (IPCC-AR4) is largest in the Arctic (Holand and Bitz, 2003). Contributing to this spread is a combination of a large inherent variability and modeling uncertainties resulting from a poor understanding of several feedback mechanisms (e.g., Sorteberg et al., 2005). The effects of Arctic clouds lie at the heart of the Arctic amplification discussion (Liu et al., 2008; Kay et al., 2008; Kay and Gettelman, 2009). Our lack of understanding of Arctic clouds and their effects greatly hinders our understanding of the Arctic climate system, and thus the ability of climate models to simulate the current climate, and to provide future projections.

Low-level clouds are ubiquitous in the Arctic, especially during the summer half of the year, with cloud fraction as large as 80–90 % (Curry and Ebert, 1992; Wang and Key, 2005; Tjernström, 2005; Shupe et al., 2005, 2011). These clouds have a substantial effect on the surface energy budget (e.g., Intrieri et al., 2002; Shupe and Intrieri, 2004; Sedlar et al., 2011a) and thus on the melting and freezing of perennial sea ice (Kay and Gettelman, 2009). Arctic clouds also present a particular problem to modeling (Walsh

Central Arctic atmospheric summer conditions during ASCOS

M. Tjernström et al.

Title Page

Abstract

Introduction

Conclusions

References

Tables

Figures



Back

Close

Full Screen / Esc

Printer-friendly Version

Interactive Discussion

et al., 2002; Tjernström et al., 2005, 2008; Karlsson and Svensson, 2010). Many global models fail to get even the annual cycle of cloud fraction correct, not to mention more subtle factors such as the altitudes and amounts of condensate in Arctic clouds (e.g., Karlsson and Svensson, 2010). In contrast to similar clouds at lower latitudes, low-level clouds in the Central Arctic tend to warm the surface relative to clear conditions most of the year (Intrieri et al., 2002; Tjernström et al., 2004a). This is due to an intricate balance between the optical properties of the clouds and a highly reflecting surface (e.g., Sedlar et al., 2011a).

Simulating clouds directly in climate models is impossible; they must be parameterized as functions of variables resolved on a coarse model grid. Developing cloud parameterizations involves theoretical considerations but ultimately relies on closure assumptions derived from observations, typically from ensembles of observational campaigns. Developing useful parameterizations requires an adequate understanding of the processes involved and testing of new cloud schemes against Arctic data. For the Arctic, such work is limited by the paucity of process-level observations and hence obtaining *in-situ* observations of clouds and cloud-related processes over the Central Arctic Ocean is crucial. Monitoring of climate in the remote Arctic must rest on remote sensing from satellites, but again there is a severe lack of in-situ observations for use in developing and testing remote sensing techniques. As a consequence, many studies are based on reanalysis data, either from regional products, such as the Arctic System Reanalysis (ASR, Bromwich et al., 2010), or global, such as for example the European Centre for Medium Range Weather Forecasts (ECMWF) ERA-Interim (Dee et al., 2011). It is sometimes easy to forget that in terms of more subtle variables and processes, output from reanalyses, while likely the best that can be done at present, is still model output. A true climatology of many such properties is still essentially absent, especially for the Arctic.

To provide the in-situ process-level data necessary to constrain or improve models several observational field programs have been conducted in the Central Arctic Ocean, but the only extensive experiment to cover a full annual cycle was the Surface Heat

Central Arctic atmospheric summer conditions during ASCOS

M. Tjernström et al.

Title Page

Abstract

Introduction

Conclusions

References

Tables

Figures



Back

Close

Full Screen / Esc

Printer-friendly Version

Interactive Discussion

**Central Arctic
atmospheric summer
conditions during
ASCOS**M. Tjernström et al.

[Title Page](#)[Abstract](#)[Introduction](#)[Conclusions](#)[References](#)[Tables](#)[Figures](#)[⏪](#)[⏩](#)[◀](#)[▶](#)[Back](#)[Close](#)[Full Screen / Esc](#)[Printer-friendly Version](#)[Interactive Discussion](#)

Budget of the Arctic Ocean (SHEBA: Uttal et al., 2002) from fall 1997 to fall 1998. The drifting Russian “North Pole” stations (e.g., Kahl et al., 1992, 1996; Serreze et al., 1992) have made many basic meteorological observations in all parts of the year but obtained few process-level observations, especially related to cloud properties. The same limitation applies for the Tara expedition during the DAMOCLES project (Gascard et al., 2008), which also covered a full annual cycle. Most other experiments have focused on the summer season, at least partly because the Arctic is reasonably accessible with icebreakers in summer.

The Arctic Summer Cloud Ocean Study (ASCOS) is the latest and most extensive in a series of expeditions with an atmospheric focus that have been deployed on the Swedish icebreaker *Oden*. The previous experiments include the International Arctic Ocean Expedition 1991 (IAOE-91, Leck et al., 1996), the Arctic Ocean Expedition 1996 (AOE-96, Leck et al., 2001) and the Arctic Ocean Experiment 2001 (AOE-2001, Leck et al., 2004; Tjernström et al., 2004a; Tjernström 2005, 2007). ASCOS was deployed in the summer of 2008, as a part of Sweden’s contribution to the 2007–2009 International Polar Year (IPY), with substantial international contributions. ASCOS was the most extensive in-situ atmospheric Arctic Ocean experiment during the IPY, lasting over a month in the North Atlantic sector of the Central Arctic Ocean. It was centered on a three-week ice-drift operation at $\sim 87^\circ$ N from mid-August through the beginning of September, with the icebreaker moored to a drifting ice floe. Figure 1 shows the track of the expedition.

Process studies such as those conducted during ASCOS must be put into a larger context. The atmosphere is highly variable on many time scales and this gives rise to two main considerations. First, any findings from process-level observations must be interpreted within the context of the larger-scale atmospheric circulation. Second, it is necessary to understand how representative observations from a short period are for climatological Arctic processes. The paucity of observations in general introduces a risk of over-interpretation of results from short field experiments. As an example the SHEBA experiment, while extensive, collected only one annual cycle of research-

quality cloud and surface flux observations. But because this is the only such data set, there is a risk they are assumed to represent a much larger area and time-frame. With an expedition as short as ASCOS this risk is obviously even greater. Therefore, new observations must be cautiously placed within the context of existing observations, e.g. satellite-based estimates or in-situ data from prior field experiments.

In this paper we present a summary of the meteorological conditions that were encountered during ASCOS, from the synoptic scale down to boundary-layer scales, to aid in interpretation of process studies presented in many other papers. In doing this, we compare the ASCOS conditions with both climatological means and with observations from three earlier summer experiments: the AOE-96, SHEBA and AOE-2001 expeditions. A brief description of ASCOS and the data used in this study is given in Sect. 2. In Sect. 3 we discuss the large-scale atmospheric setting and transport characteristics during ASCOS, while Sect. 4 presents some basic meteorological characteristics from ASCOS, comparing these to results from the other experiments. Section 5 describes some of the main characteristics of the ASCOS ice drift and Sect. 6 contains a brief summary and conclusions.

2 Data

2.1 The ASCOS experiment

The primary objective of ASCOS is to understand the formation and life cycle of low-level clouds and the role these play in the surface energy budget of the high Arctic, especially during the transition from late summer to early fall. ASCOS was designed as an interdisciplinary project with science teams specializing in meteorology, physical oceanography, atmospheric gas-phase chemistry, particulate chemistry and physics, marine biology and biochemistry. Like its predecessors (IAOE-91, AOE-96 and AOE-2001), ASCOS was conducted onboard the Swedish icebreaker *Oden*. The expedition

Central Arctic atmospheric summer conditions during ASCOS

M. Tjernström et al.

Title Page

Abstract

Introduction

Conclusions

References

Tables

Figures

◀

▶

◀

▶

Back

Close

Full Screen / Esc

Printer-friendly Version

Interactive Discussion

departed Longyearbyen on Svalbard on 2 August (DoY¹ 214), returning on 9 September (DoY 253), 2008. By 12 August (DoY 225), after a few brief research stations in open water and the marginal ice zone and a transit north into the pack ice, *Oden* was moored to a 3 × 6 km ice floe with which it drifted for 21 days. The drift track, from approximately 87°21' N, 01°29' W to 87°09' N, 11°01' W, is illustrated in Fig. 1. A detailed summary of the scientific background and details on all observations is contained in Tjernström et al. (2011) and only a brief summary will be provided here.

Operational large-scale meteorological analysis and forecasts for the expedition were supplied by the European Centre for Medium Range Weather Forecasts (ECMWF) and the UK Met Office; in this paper we use the ECMWF analyses while the UK Met Office Unified Model forecasts are presented and analyzed in Birch et al. (2011). To compare ASCOS conditions to climatology we use the NCAR/NCEP reanalysis products, readily available from the National Oceanographic and Atmospheric Administration/Earth System Research Laboratory (NOAA/ESRL) web-site at <http://www.esrl.noaa.gov/psd>. Back-trajectories based on analyzed meteorological fields calculated after the expedition, were obtained from HYSPLIT (<http://ready.arl.noaa.gov/HYSPLIT.php>).

Table 1 summarizes the different sources of data from all four expeditions used in this study. For ASCOS, basic meteorology parameters were extracted from *Oden's* weather station, complemented by a WeatherPak installed onboard providing some redundancy, and from the micro-meteorology deployment on the ice during the ice drift. Analyses of tropospheric vertical structure, clouds and frontal zones rest on the 6-hourly radiosoundings and on the MilliMeter wave-length Cloud Radar (MMCR) installed on the *Oden*. Additional information on the clouds comes from several laser ceilometers, and additional temperature profile information comes from a scanning microwave radiometer. Visibility is provided by a backscatter visibility sensor that was part of the *Oden* weather station. Observations of surface radiation fluxes come from

¹Throughout ASCOS, time is usually given as decimal day-of-the-year (DoY), defined so that DoY = 1.0 occurs at 00:00 UTC on 1 January.

**Central Arctic
atmospheric summer
conditions during
ASCOS**

M. Tjernström et al.

Title Page

Abstract

Introduction

Conclusions

References

Tables

Figures



Back

Close

Full Screen / Esc

Printer-friendly Version

Interactive Discussion



Discussion Paper | Discussion Paper | Discussion Paper | Discussion Paper | Discussion Paper

broadband pyranometers and pyrgeometers deployed on the ice, complemented by similar instruments on the *Oden*; net surface radiation could only be measured on the ice. Turbulent heat fluxes were derived from eddy-correlation measurements made on two micrometeorology masts on the ice. Several other instrument systems were also deployed during ASCOS (see Tjernström et al., 2011, for a complete description) but are not used here.

2.2 Previous expeditions

Data from other expeditions are used to put ASCOS results into a broader context. This data comes from the AOE-96, SHEBA and AOE-2001 experiments (see Leck et al., 2001; Uttal et al., 2002; Tjernström et al., 2004a,b, respectively, for descriptions). ASCOS and the previous *Oden*-based expeditions were of limited length and for different, but overlapping, periods, while SHEBA was deployed for a full year. The overlapping time period for all expeditions is only 4–23 August, about three weeks. Directly comparing observations from four different years for such a brief period of time is difficult and perhaps not even meaningful. For this reason we instead consider the statistics of the different observations, rather than comparing individual time series.

With a primary interest in conditions during late summer and the early transition to autumn, we use *all* available observations within the perennial pack ice from the months of July and August from each experiment; this paper focuses on ASCOS so we extend the period 1 full day into September to include the end of the ASCOS ice drift. In summary, we use all available observations made within the perennial pack ice between 00:00 UTC on 1 July and 00:00 UTC on 2 September. A consequence of using different time periods is that some of the observations are biased towards the mid-summer melt period (e.g., SHEBA), while other may be dominated by the fall transition (e.g., ASCOS and AOE-96). Figure 2, showing the near-surface temperature records for all four expeditions, illustrate the time overlap of the expeditions. ASCOS, as well as AOE-96 and AOE-2001, were deployed in the North Atlantic sector of the Arctic Ocean, while SHEBA was deployed in a different region, substantially farther

Central Arctic atmospheric summer conditions during ASCOS

M. Tjernström et al.

Title Page

Abstract

Introduction

Conclusions

References

Tables

Figures



Back

Close

Full Screen / Esc

Printer-friendly Version

Interactive Discussion



south (Fig. 1).

As far as possible we have used the same, or similar, types of observations to compare different parameters; see Table 1. However, for some parameters data is not available from all expeditions. In these cases the missing expedition is simply omitted.

In other cases, different types of observations or sensors were used for the same basic purpose. For example, cloud observations in SHEBA and ASCOS were obtained from the MMCR cloud radar, AOE-2001 deployed an S-band cloud and precipitation radar, while AOE-96 had no cloud radar. Also, while ASCOS, SHEBA and AOE-2001 had substantial ice drifts, AOE-96 had a very short ice-drift and data from the latter is omitted. The number of soundings included in the comparison differs, and there has been a significant development in radiosonde sensor technology between 1996 and 2008. Thus, differences in time, frequency and quality of the observations, must be born in mind during the following analysis. It is not the intention of this paper to establish a “summer Central Arctic climatology”. However, we do believe that some similar characteristic have been observed.

3 Large-scale atmospheric setting during ASCOS

Figure 3 shows the mean sea-ice area cover from the National Snow and Ice Data Center (NSIDC) for August of each experimental year. The general trend is of decreasing summer sea ice extent with time: 1996 had the largest total area cover and 2008 the smallest. There are also interannual differences in the regional location of the pack ice. For example, the ice edge was far north in the Alaskan/East-Siberian sector during 1998 (the SHEBA summer) and again in 2008, while being farther south in 1996 and 2001. The ice fraction around the pole is lowest in 1996, consistent with reports of many open leads (Leck et al., 2001), and low again in 2008.

The synoptic-scale atmospheric circulation exhibits large interannual variability, thus before examining detailed observations from a limited time it is useful to compare prevailing conditions to climatology using reanalysis products. Figure 4 shows the main

Central Arctic atmospheric summer conditions during ASCOS

M. Tjernström et al.

Title Page

Abstract

Introduction

Conclusions

References

Tables

Figures

⏪

⏩

◀

▶

Back

Close

Full Screen / Esc

Printer-friendly Version

Interactive Discussion



**Central Arctic
atmospheric summer
conditions during
ASCOS**

M. Tjernström et al.

Title Page

Abstract

Introduction

Conclusions

References

Tables

Figures

⏪

⏩

◀

▶

Back

Close

Full Screen / Esc

Printer-friendly Version

Interactive Discussion



features of the large-scale atmospheric circulation during ASCOS, as manifested by the mean-sea-level pressure (MSLP) and the 850 and 500 hPa geopotential height fields (Fig. 4a–c) and their anomaly compared to the 1981–2010 climatology over the same time period (Fig. 4d–f). The MSLP (Fig. 4a) features a high-pressure region over the North-American and Siberian quadrants with a center over the Canada Basin and a separate high-pressure center over Greenland. Low pressure centers are located over the Barents and Nordic Seas and over the Canadian Archipelago. While the Greenland high-pressure center is consistent with the climatology, the pressure pattern over the Arctic Ocean is anomalous (Fig. 4d), with a positive anomaly of up to 5–6 hPa over the Canada Basin and a similar negative anomaly over the Barents Sea. This implies an easterly surface-flow anomaly over much of the ASCOS region, which is consistent with the more detailed synoptic-scale analysis below. The low-pressure region remains at approximately the same horizontal location in the vertical while broadening somewhat across Northern Greenland and the high-pressure region moves gradually westward in over Siberia with altitude. The anomaly is thus nearly barotropic in character and exhibits about the same spatial structure on both pressure surfaces (Fig. 4e,f), while the pressure field itself is baroclinic.

Figure 5 shows the temperature fields and its anomalies. The region with the lowest temperature tilt with height across the Arctic from the Beaufort Sea at the surface, centered on the North Pole at 850 hPa and located north of Svalbard at 500 hPa. The temperature anomaly displays a dipole pattern with high near-surface temperatures over Greenland and Siberia, marginally low temperatures on the Canadian side of the Arctic Ocean, but a bridge of positive temperature anomaly from Greenland to Siberia strengthening with altitude. Precipitable water (Fig. 6) is high over Siberia and low over Greenland; the high values over Siberia are an anomaly while conditions over Greenland are only marginally moister than climatology. At the surface the relative humidity is the highest north of North America and Greenland, corresponding to climatology, while the anomaly field shows drier than average conditions in a band from north of the Bering Strait along the Siberian coast to the Kara Sea.

**Central Arctic
atmospheric summer
conditions during
ASCOS**M. Tjernström et al.

[Title Page](#)[Abstract](#)[Introduction](#)[Conclusions](#)[References](#)[Tables](#)[Figures](#)[⏪](#)[⏩](#)[◀](#)[▶](#)[Back](#)[Close](#)[Full Screen / Esc](#)[Printer-friendly Version](#)[Interactive Discussion](#)

Figure 7 illustrates details of the synoptic scale weather during ASCOS. A select set of ECMWF surface pressure and wind analyses are shown, complemented by 12-hourly storm tracks for the most significant weather systems. During the first part of the expedition several significant storms moving from east to west passed the ASCOS track, the opposite of the usual direction of travel and consistent with the MSLP anomalies (Fig. 4d). Figure 7a shows the first, starting on 4 August (DoY 217) in the Canada basin, moving to the Kara Sea by 7 and 8 August (DoY 220 and 221), crossing over Svalbard on 10 August and then passing ASCOS on 12 August (DoY 225). This was the first day of the ice drift and this weather system slowed down the initial deployment of instrumentation on the ice, bringing strong winds, precipitation and generally adverse conditions for working on the ice.

The next weather system (Fig. 7b) started on 12 August (DoY 225) over the Kara Sea and then moved rapidly westwards passing south of the ASCOS ice drift on 14 and 15 August (DoY 227 and 228) and dissipated north of the Canadian Archipelago. The flow then changed character, with two storms passing rapidly eastward across the Nordic, Greenland and Kara Seas without affecting ASCOS. After this, the synoptic-scale weather became more quiescent, with the formation of a high-pressure system over Svalbard (Fig. 7c,d), which moved slowly towards and across the North Pole. A secondary high pressure over Greenland created a common omega-shaped blocking pattern over the North Atlantic. Towards the end of the ice drift an extensive and intense low-pressure system developed over the Kara Sea and moved westward towards Svalbard (Fig. 7d). This did not affect the ASCOS observations until after the ice drift had been terminated and the *Oden* was moving south in the open Greenland Sea towards Longyearbyen.

Figure 8 shows back-trajectories with receptor points at the location of *Oden* at 100, 500 and 2000 m above the surface, respectively. These heights were selected with aerosol processes in mind, the lowest and highest being within the boundary layer and in the free troposphere, respectively, while the 500-m level was expected to be roughly in the cloud layer. Although the variability is large, five broad flow regimes can

be identified. Early in the expedition, while *Oden* was moving north towards and into the ice (4–9 August; DoY 217–222) the air approaching ASCOS predominantly arrived from the ice covered region north of Canada and Alaska. Conditions then changed and during 9–20 August (DoY 222–233) the origin of the air was highly variable on a daily time scale but mostly came from the Greenland, Barents and Kara Seas; this was the synoptically very active period discussed above (see Fig. 7a,b). A new shift occurred around 20 August (DoY 233), with a period when trajectories reaching ASCOS mostly originated in the vicinity of Greenland. Through the end of the ice drift and the beginning of the traverse back to the Greenland Sea (28 August–4 September; DoY 241–248) the origin of the air swings around to come from across the Central Arctic. At the end of the campaign (DoY 248–251), the origin of the air was again from the Kara Sea and adjacent land. Many of these shifts are clearly distinguishable in the observations.

Figure 9 shows a subjective analysis of passing frontal disturbances associated with the synoptic-scale weather systems, overlaid onto both the MMCR cloud radar reflectivity (Fig. 9a) and the equivalent potential temperature², Θ_e , from the soundings (Fig. 9b). The dashed vertical lines indicate the beginning and end of the ice-drift period. The subjective analysis is produced using the time-rate-of-change and the slope with height of Θ_e , aided by the MMCR cloud reflectivity. The most intensive period of weather systems is roughly from 6 through 21 August (DoY 219–234). The most significant set of fronts is associated with the synoptic scale disturbance that arrived on 12 August (DoY 225). This period ended with a weather system on 20 August (DoY 233), followed by a two day period with only low-level cloud or fog which ended on 23 August (DoY 236) with another weather system; depending on definition either of these

² $\Theta_e = \Theta + \frac{L\Theta}{c_p T} q$, where Θ is the potential temperature defined as $\Theta = T(\rho/1000)^{\frac{R_d}{c_p}}$, T is the temperature, ρ is the pressure, R_d and c_p are the gas constant and heat capacity of dry air, respectively, L is the latent heat of vaporization and q is the specific humidity. Note that the temperature (T) in the definition of Θ_e is evaluated at the lifting condensation level in unsaturated conditions.

**Central Arctic
atmospheric summer
conditions during
ASCOS**

M. Tjernström et al.

Title Page

Abstract

Introduction

Conclusions

References

Tables

Figures

⏪

⏩

◀

▶

Back

Close

Full Screen / Esc

Printer-friendly Version

Interactive Discussion



weather systems marked the end of the melt season (Sedlar et al., 2011a; Sirevaag et al., 2011; , Persson et al 2012); see Sect. 5. Thereafter follows a more quiescent period from 23 August through 3 September (DoY 236–247) under the influence of a high-pressure system with several embedded weak frontal passages; favorable conditions for a persistent stratocumulus layer residing in the subsidence inversion. Following this, synoptically more active weather reappears as ASCOS nears its end. The different periods observed during the ice drift will be discussed in detail in Sect. 5.

4 Meteorological conditions encountered during ASCOS

4.1 Basic meteorological variables

In this section we present key meteorological variables from ASCOS. A comparison to observations from earlier expeditions is included to put ASCOS results in context. Figure 2 shows time series of near-surface temperature from the four expeditions. Near-surface temperature during July (DoY 183–213) remains close to 0 °C, as expected for the melt season, when all excess heating contributes to melting of ice and snow rather than to a surface warming. Through August (DoY 212–243) all four time series show a gradual decrease in temperature with time, along with the occurrence of brief colder periods lasting for up to several days. These periods appear to be a common feature, perhaps signaling the oncoming transition to fall freeze-up conditions, and have been associated with periodic breaks or reductions in cloud cover (Tjernström, 2005; Sedlar et al., 2011a).

Figure 10 shows the relative probability of near-surface temperature, relative humidity and wind speed. In generating these statistics from the three *Oden*-based expeditions, we used both the ship's weather station and observations made on the ice during the ice-drifts (absent for AOE-96). For SHEBA we used only observations from the mast on the ice (e.g., Persson et al., 2002). The *Oden* weather station was located at ~20 m above the ice, while the height of the observations made on the ice varies

Central Arctic atmospheric summer conditions during ASCOS

M. Tjernström et al.

Title Page

Abstract

Introduction

Conclusions

References

Tables

Figures



Back

Close

Full Screen / Esc

Printer-friendly Version

Interactive Discussion



between the expeditions, generally in the 5–15 m interval.

Temperatures during ASCOS were mostly in the -2 to 0°C range, which is roughly the interval between the freezing points of saline (ocean) water and fresh (snow on top of the ice) water and is typical for the melt season. The ice-drift measurements also clearly reflect the two periods of lower temperatures around DoY 235 and 245. The statistics from the other four expeditions are very similar. The temperatures from SHEBA are the warmest and peak at a slightly positive temperature, while those from AOE-96 are the coolest, with a broad peak around $\sim -1.5^{\circ}\text{C}$. All distributions have a negative tail, SHEBA the least and ASCOS and AOE-96 the most. These are a reflection of the temporary drops in temperature that predominantly appeared in August. The fact that SHEBA is somewhat warmer is a consequence of including the whole month of July, which is somewhat warmer on average; SHEBA is also at a more southerly location. Leck et al. (2001) report that AOE-96 was an unusually cloud free and attribute the cooler temperatures to the lack of positive cloud radiative forcing. The ASCOS near-surface conditions were also very moist (Fig. 10b), with the most commonly occurring near-surface relative humidity close to 100 %, and almost no cases where it dropped below 90 %. ASCOS conditions fall in the middle of these expeditions with SHEBA, followed by AOE-2001, being the most humid. AOE-96 is again slightly different, with somewhat lower relative humidity peaking at 96 %, consistent with the lower clouds amounts and thus cooler temperatures.

The wind speed does not have any constraints similar to that for temperature and moisture, and is consequently more variable. For ASCOS the winds were significantly weaker when considering only the ice drift than for the whole expedition (Fig. 10c). This is a manifestation of the generally more synoptically active period at the beginning of the expedition, ending a few days into the ice drift. The most common wind speeds for the whole expedition were $3\text{--}5\text{ m s}^{-1}$, with a weak secondary peak at 10 m s^{-1} and no cases of winds $> 16\text{ m s}^{-1}$. The ice drift was significantly calmer with winds mostly $1\text{--}4\text{ m s}^{-1}$ and very few cases of winds $> 5\text{ m s}^{-1}$. The tower observations from ASCOS, AOE-2001 and SHEBA were made using sensors at a lower height than those

**Central Arctic
atmospheric summer
conditions during
ASCOS**

M. Tjernström et al.

Title Page

Abstract

Introduction

Conclusions

References

Tables

Figures



Back

Close

Full Screen / Esc

Printer-friendly Version

Interactive Discussion



made on the ship. A comparison of ship-borne and mast-borne measurements from ASCOS, only using data from periods when they coexist, suggests that the height of the measurement makes only a small difference (not shown). Comparing the expeditions, the SHEBA record has the lowest winds, while AOE-2001 has the highest, with ASCOS in between. The peak in the AOE-96 statistics is similar to that from SHEBA, but there is also a secondary peak at higher wind speeds. In general, across all the expeditions, wind speeds were commonly $2\text{--}8\text{ m s}^{-1}$, seldom above 10 m s^{-1} and hardly ever exceeding 15 m s^{-1} .

4.2 Vertical structure

The vertical thermodynamic structure of the lower atmosphere ($< 4\text{ km}$) was evaluated from the radiosoundings. Figure 11 shows the probability of equivalent potential temperature, Θ_e , as a function of altitude. A constant value with height signifies near-neutral moist-static stability conditions, while increasing values are statically stable. Figure 12 shows similar statistics for relative humidity (RH). A dominating feature from ASCOS was a pronounced near-neutrally stratified layer in the lowest atmosphere, from the surface up to $\sim 500\text{ m}$ (Fig. 11a), accompanied with high relative humidity, generally $\text{RH} > 95\%$, in a layer from the surface up to about 1 km (Fig. 12a). This is consistent with the observation that specific humidity increases across the boundary-layer inversion (Tjernström et al., 2004a; Tjernström, 2005; Devasthale et al., 2011). With increasing temperature with height, if the relative humidity is constantly high, it follows that as temperature increases into the inversion specific moisture must also increase. It also suggests the possibility that clouds may penetrate into the lower inversion, rather than being capped by it. This structure has been found to be common in cloud radar and temperature profiles from AOE-2001, ASCOS, SHEBA and Barrow, Alaska (Sedlar and Tjernström, 2009; Sedlar et al., 2011b), and recognized as important for the persistence of Arctic stratocumulus clouds (Solomon et al., 2011).

The vertical structure in the three other experiments is strikingly similar to ASCOS, although details differ. The depth of the near-neutrally stratified layer in the lowest

Central Arctic atmospheric summer conditions during ASCOS

M. Tjernström et al.

Title Page

Abstract

Introduction

Conclusions

References

Tables

Figures

◀

▶

◀

▶

Back

Close

Full Screen / Esc

Printer-friendly Version

Interactive Discussion



atmosphere ranged from 300–400 m in AOE-2001 and AOE-96 to ~ 400 m during SHEBA (Fig. 11b–d); ASCOS thus featured the deepest neutrally stratified layer. During ASCOS (Fig. 11a) well-mixed surface layers appeared preferentially at two temperatures, around $\Theta_e \sim 9^\circ\text{C}$ and at a lower temperature of $\Theta_e \sim 3^\circ\text{C}$. A similar feature, although weaker, was present also in AOE-96 (Fig. 11c). In both cases the colder structures were shallower. During AOE-96 and SHEBA, the boundary-layer temperature was slightly lower, at $\Theta_e \sim 7\text{--}8^\circ\text{C}$. All the expeditions also had very high relative humidity in the lowest troposphere, $> 95\%$ (Fig. 12b–d). The highest relative humidity was observed during SHEBA, being even higher than during ASCOS (Fig. 12a,d), while the lowest values were found in AOE-2001 (Fig. 12b). The moist layer is also deeper than the well-mixed layer for all expeditions often reaching to > 1 km. SHEBA had the deepest moist layer, slightly deeper than ASCOS, while AOE-96 had the most shallow layer, ~ 500 m. The lower troposphere stratification is thus very similar in all four expeditions.

The characteristics of the capping inversion are illustrated in Fig. 13, showing the base height of the capping inversion, and its thickness, strength and static stability. This analysis is based on scanning radiometer temperature profiles from ASCOS and AOE-2001, and on radiosoundings for SHEBA. The objective algorithm applied to the temperature profiles to determine the inversions is that of Tjernström and Graversen (2009); the main inversion is defined as that with the strongest stability and there is a very clear correlation between strength, stability and depth (not shown). Note that with this data, inversions with a base below but a top above 1.2 km (the maximum height of the scanning radiometer) will be represented in the inversion base statistics, but not in the statistics for thickness and strength. Over 95% of all analyzed profiles feature at least one main inversion (e.g., Tjernström 2005, 2007; Tjernström and Graversen, 2009) and multiple inversions in the lowest kilometer were common. The absolute peak in the probability for the height to base of the main inversion (Fig. 13a) in ASCOS occurred at ~ 100 m, however, for the rest of the altitude interval the probability function is fairly flat, indicating that high as well as low inversions were occurring

**Central Arctic
atmospheric summer
conditions during
ASCOS**

M. Tjernström et al.

Title Page

Abstract

Introduction

Conclusions

References

Tables

Figures



Back

Close

Full Screen / Esc

Printer-friendly Version

Interactive Discussion



about at about the same frequency. The thickness of ASCOS inversion were most often around 100–300 m, and the probability function for inversion strength was broad, $\Delta T \sim 1\text{--}6^\circ\text{C}$.

Comparing to other expeditions, both SHEBA and AOE-2001 had more distinct low-level peaks for the inversion base heights with AOE-2001 somewhat higher, at ~ 200 m, and SHEBA slightly lower. In neither of these were there any significant occurrences of inversion bases above ~ 800 m. Both SHEBA and AOE-2001 had more occurrences of thicker inversions, with a broader peak from 100 to 600 m (Fig. 13b), and while AOE-2001 had significantly more weak inversions with pronounced peak at $\Delta T \sim 1^\circ\text{C}$ (Fig. 13c), SHEBA had similar inversion strengths compared to ASCOS. Inversions never exceed $\Delta T \sim 12^\circ\text{C}$ in any of the expeditions. In terms of stability, combining the strength and depth for the individual inversions (Fig. 13d), ASCOS and SHEBA were very similar, while AOE-2001 inversions had significantly weaker stability.

Figure 14 shows median profiles of temperature, specific humidity and wind speed for all four expeditions. The median temperature profiles (Fig. 14a) exhibited a well-mixed near-surface layer, the deepest during ASCOS and shallowest in AOE-2001, capped by an inversion – strongest and deepest in AOE-2001 and weakest and highest during ASCOS while AOE-96 and SHEBA are very similar. AOE-96 also had a slightly higher stability near the surface. The specific humidity (Fig. 14b) varied considerably between the expeditions and is the lowest in AOE-96, consistent with the subjective impressions of less clouds and cooler conditions in AOE-96. SHEBA was moistest, with a significant layer of higher values between ~ 400 m and ~ 1.2 km.

Wind speeds in the lower troposphere, below 1–2 km, were highest during AOE-96 ($\sim 8\text{ m s}^{-1}$) and the lowest in AOE-2001 ($\sim 5\text{ m s}^{-1}$) with ASCOS and SHEBA being similar at $\sim 6\text{ m s}^{-1}$ (Fig. 14c). AOE-96, and possibly ASCOS, had weak low-level wind speed maxima between 100 m and 1 km indicating the presence of low-level jets; SHEBA and AOE-2001 had no such signal although varying heights, strengths and occurrences may have obscured those in the median profile. The most striking difference in wind speeds is, however, found in the upper troposphere, where all three

Central Arctic atmospheric summer conditions during ASCOS

M. Tjernström et al.

Title Page

Abstract

Introduction

Conclusions

References

Tables

Figures



Back

Close

Full Screen / Esc

Printer-friendly Version

Interactive Discussion

Oden-based expeditions encountered significantly higher median wind speeds than did SHEBA, at 15–20 m s⁻¹ and ~ 10 m s⁻¹, respectively, with ASCOS having the highest values. Although the sample is very small, such a difference may be a consequence of the differences in location. In this upper-troposphere layer ASCOS also had the highest and AOE-96 the second lowest wind speeds, with AOE-2001 in between. Assuming that the wind-speed increase with height across the troposphere is a proxy for baroclinic instability, these differences might reflect differences in synoptic-scale activity between the two regions, the Beaufort Sea for the SHEBA deployment and the Atlantic sector of the Central Arctic where the *Oden*-based expeditions were deployed, and differences between the different years in the latter.

4.3 Clouds

For the purpose of this study, “a cloud” is defined by the instruments used for detecting it (see discussion in Shupe et al., 2011). For ASCOS and AOE-2001 cloud fractional occurrence was estimated using ceilometer data, while during SHEBA cloud-occurrence statistics was estimated using a multi-sensor approach, including lidar and cloud radar. With this in mind, ASCOS and AOE-2001 cloud occurrence fractions might be underestimated since they use only a single sensor with lower sensitivity at higher altitudes. Note also that cloud fraction is defined using zenith-viewing instruments, sensing clouds as a function of time as they pass above, and thus not estimating the actual spatial cloud cover at any given time.

Several studies have indicated large amounts of low-level cloud in the Arctic during summer (e.g., Wang and Key, 2005; Karlsson and Svensson, 2010). For ASCOS the average total cloud fraction was about 90 % while the boundary layer cloud fraction was about 80 %. During AOE-2001 the average total cloud cover was 85 %, and 80 % for boundary-layer clouds. Shupe et al. (2011) reports a mean cloud fraction from 90 to close to 100 % from SHEBA, for July and August, respectively.. Cloud fraction was not estimated objectively for AOE-96.

Central Arctic atmospheric summer conditions during ASCOS

M. Tjernström et al.

Title Page

Abstract

Introduction

Conclusions

References

Tables

Figures



Back

Close

Full Screen / Esc

Printer-friendly Version

Interactive Discussion



**Central Arctic
atmospheric summer
conditions during
ASCOS**M. Tjernström et al.

[Title Page](#)[Abstract](#)[Introduction](#)[Conclusions](#)[References](#)[Tables](#)[Figures](#)[⏪](#)[⏩](#)[◀](#)[▶](#)[Back](#)[Close](#)[Full Screen / Esc](#)[Printer-friendly Version](#)[Interactive Discussion](#)

Figure 15 shows statistics of cloud geometry. Here the cloud base is defined by the lowest indication of a cloud from the ceilometer or the cloud radar, whichever is the highest, while the cloud top is obtained from cloud radar. For SHEBA, only occurrences with single-layer clouds are used. These totally dominated in August; in July single-layer clouds were the most common, while there were more cases with multiple cloud layers (Intrieri et al., 2002). The height of the lowest cloud base (Fig. 15a) has a pronounced low-level maximum in all four experiments, peaking at < 100 m, while the lowest cloud tops (Fig. 15b) usually occur below 1 km, with a maximum between 200 and 800 m for the three *Oden* expeditions. SHEBA also has a secondary peak of lowest cloud-top around ~ 1 km. Figure 15c shows statistics of estimated cloud thickness: for ASCOS and AOE-2001 this has a maximum around 300 m, with very few clouds thicker than 1 km. SHEBA has a more uniform distribution between 300 m and ~ 1 km.

ASCOS and SHEBA carried passive dual-wavelength microwave radiometers that continuously monitor vertically-integrated column water vapor (precipitable water) and liquid water path, the vertically integrated cloud water content (Westwater et al., 2001). Both expeditions also deployed the MMCR cloud radar, facilitating an estimate of integrated cloud ice (Shupe et al., 2005). Figure 16 shows these three measures for ASCOS and SHEBA. The total column water vapor distributions (Fig. 16a) are very similar, with the SHEBA results shifted to somewhat moister conditions, possibly a consequence of SHEBA's more southerly location. In terms of cloud water (Fig. 16b,c), ASCOS has significantly more cloud liquid than SHEBA but less cloud ice.

Figure 17 shows the probability distribution of the visibility from the backscatter visibility sensor; for SHEBA this information is not available. All three exhibit similar behavior, with peaks below 1 km (the threshold for fog conditions according to the WMO definition) and for visibility > 20 –30 km. Note that visibility can also be low in snowfall, when fog is normally dissipated. Visibility less than 1 km was most common during ASCOS (25 % of the time) and somewhat less during the other expeditions (10–15 %). The relative lack of visibility observations in the 1–10 km range indicates that haze conditions, caused by the uptake of water on hygroscopic aerosols at relative humidity

< 100 %, was essentially non-existent.

4.4 Surface energy fluxes

Incoming (downward) long- and shortwave radiation is strongly affected by clouds and was observed onboard the ship during the three *Oden* expeditions, on the ice during the AOE-2001 and ASCOS ice-drifts, and continuously on the ice during SHEBA. The upward radiative fluxes (and thus net fluxes) are only available from observations on the ice.

During ASCOS the incoming solar radiation (Fig. 18a) peaked at approximately 50–100 W m⁻² from both the longer ship record and the observations from the ice, with very few values > 200 W m⁻². For net solar radiation at the surface (Fig. 18b) the distribution from ASCOS had a sharp peak at ~ 10 W m⁻², with few values > 50 W m⁻². Incoming longwave radiation (Fig. 18c) had a peak around 300–310 W m⁻² with a sharper somewhat lower peak when considering only the ice drift. There was a long tail towards lower values, down to 200–220 W m⁻². The net longwave radiation had a sharp peak at -10 W m⁻² with a negative tail down to ~ -60 W m⁻². This behavior with quite distinct peaks and long tails is a result of the impact of the clouds on the radiation; the peaks represent the usually cloudy conditions while the tails, negative for net longwave and positive for net shortwave, reflects the relatively few and short clear periods.

Comparing to the other expeditions, there are similarities and some differences. Incoming solar radiation for the longer ship record at AOE-2001 peaked at 140 W m⁻², while its ice drift probability peaked at slightly lower values, at ~ 100 W m⁻², and the distribution was narrower. AOE-96 had peak values similar to ASCOS, but with a wider distribution, while SHEBA conditions had a much wider distribution with a flat peak around 10–80 W m⁻² and a long positive tail. For net solar radiation at the surface (Fig. 18b) the distributions from ASCOS and AOE-2001 were similar but with higher peak values for AOE-2001 by about 10 W m⁻²; both had similar tails with few values > 50 W m⁻². SHEBA was again different, peaking at ~ 10 W m⁻² and exhibiting a broad distribution that tapered off at > 100 W m⁻². The SHEBA observations stand out; it was

Central Arctic atmospheric summer conditions during ASCOS

M. Tjernström et al.

Title Page

Abstract

Introduction

Conclusions

References

Tables

Figures

⏪

⏩

◀

▶

Back

Close

Full Screen / Esc

Printer-friendly Version

Interactive Discussion



located farther south and had a smaller LWP than ASCOS (Fig. 16b), both of which contribute to higher incoming solar radiation. In addition to a lower LWP, SHEBA had significantly more melt ponds during summer than at both AOE-2001 and ASCOS, likely causing a lower surface albedo. The incoming longwave radiation (Fig. 18c) was more similar across the four expeditions, with peaks in the 300–320 W m⁻² range, SHEBA being marginally higher, while the larger occurrence of lower values in AOE-96 reflects more clear conditions. The same is true also for net longwave (Fig. 18d), with peaks around -10 to 0 W m⁻². SHEBA had a somewhat broader distribution and an absolute peak at a few W m⁻² (positive), and more frequent occurrences of values in the -10--20 W m⁻² range.

Turbulent surface heat fluxes in the Arctic are generally small (e.g., Persson et al., 2002; Tjernström, 2005). In Fig. 19a,b statistics of the turbulent surface energy fluxes for ASCOS are compared to AOE-2001 and SHEBA; upward fluxes are defined positive. The sensible heat flux (Fig. 19a) during the ASCOS ice drift had a sharp peak in probability around zero, with both positive and negative tails. The positive tail was the more substantial, up to 10 W m⁻², while the negative tail, down to -5 W m⁻², was less pronounced. The distributions for the AOE-2001 and SHEBA sensible heat fluxes were quite similar, peaking around zero, and the tails were more pronounced and evenly distributed, ±7–8 W m⁻², compared to ASCOS.

The latent heat flux time series are shorter because of difficulties in measuring the flux in the Arctic among other things owing to accumulation of ice frost and riming on the optical surfaces of the open path sensors used in all these experiments. As this would occur mostly in cases with a downward directed flux of water vapor, exclusion of such episodes may have biased the result. ASCOS and SHEBA fluxes were mostly positive (Fig. 19b) indicating that evaporation is most common, although maximum values are small, ~ 5 W m⁻². AOE-2001 has more cases with a downward latent heat flux, although upward fluxes still dominate. Near zero fluxes dominate during all three expeditions. Figure 19c shows the bulk temperature gradient across meteorological masts, as a simple measure of stability. These are computed over slightly different

**Central Arctic
atmospheric summer
conditions during
ASCOS**

M. Tjernström et al.

Title Page

Abstract

Introduction

Conclusions

References

Tables

Figures

⏪

⏩

◀

▶

Back

Close

Full Screen / Esc

Printer-friendly Version

Interactive Discussion

height intervals, depending on the deployment of the instruments (within 8–15 m above the surface). These are relatively similar for all expeditions, with near-neutral conditions being the most common. ASCOS was more frequently unstably stratified than AOE-2001 or SHEBA, consistent with the sensible heat flux (Fig. 19a).

5 Characteristics of the ASCOS ice drift

The ice drift of ASCOS took place roughly between 00:00 UTC 13 August (DoY 225) and 00:00 UTC 2 September (DoY 246), although different instrument systems came on line gradually over the first few days, and the tear-down progressively reduced instrumentation during the last day. The effective length of the ice drift is illustrated in Fig. 20a showing time series of several temperatures near the surface (air temperature at 3.2 m and a set of surface temperatures). Sedlar et al. (2011a) analyzed the surface energy budget and defined four main periods for the ice drift with different characteristics; here we refine these definitions and additionally divide their first period into two for a total of five periods, which are discussed below and in Figs. 20–24.

Figure 20a shows that the first two periods were somewhat typical for the melt season. Both had a significant excess of surface energy, as analyzed by Sedlar et al. (2011a), that could melt ice and snow at the surface, however, the 1st period was significantly more variable in temperature than the second. Figure 20b shows the cloud radar reflectivity and reveals a more synoptically active 1st period compared to the 2nd, although both were affected by several weather systems as manifested by the deep frontal cloud structures, especially 12–13 and \sim 16 August (DoY 225–226 and 229), with three more minor systems in between. Both periods have a high cloud fraction within the lowest kilometer and also a significant amount of higher cloud, the 1st period more so than the 2nd.

A weather system at the end of the 2nd period (20 August; DoY 233) marks the end of the typical melt-season conditions and is followed by a 3rd period, which saw mostly low-level clouds and fog and the temperature falls to $\sim -6^{\circ}\text{C}$ for approximately

Central Arctic atmospheric summer conditions during ASCOS

M. Tjernström et al.

Title Page

Abstract

Introduction

Conclusions

References

Tables

Figures



Back

Close

Full Screen / Esc

Printer-friendly Version

Interactive Discussion



2.5 days (Fig. 20a). Relatively large cloud fractions were associated with this period, although clouds were mostly limited to below 400–500 m. The cloud fraction aloft mostly remained below 30 % with a slight increase around 6–8 km due to the optically thin cirrus cloud seen in Fig. 20b during this period. The surface albedo first increased due to fresh snow from the weather system on the 20th. During the 3rd period, freezing of melt ponds and some of the open (saline) water surface, along with heavy riming and frost deposits, increased the surface albedo further (Sedlar et al., 2011a). A weather system on 23 August (DoY 236) additionally covered the surface with a layer of new snow. The transmission of solar radiation through the ice also went through an abrupt change on 24 August (Sedlar et al., 2011a; Sirevaag et al., 2011); this also ended the 3rd period. The surface albedo increased from ~ 70 % to ~ 85 % from before to after the 3rd period (not shown) and the surface energy balance did not recover to positive values again.

Surface temperature remained around the freezing point of ocean salt water during the whole 4th period (approximately -2°C , Fig. 20a). This period was characterized by relatively steady conditions, with a significant diurnal cycle in near-surface temperature that now became possible because the variations in surface temperature are not limited by the melting point of fresh water. Conditions were governed by a quasi-steady high-pressure system (see Fig. 7d), and the dominating feature was a persistent stratocumulus layer. The 4th period thus had a high cloud fraction below 1 km, and approximately 10% cloud cover on average in the free troposphere (Fig. 20b). The clouds contributed to the maintenance of the surface energy balance close to zero through surface cloud-radiative forcing (Sedlar et al., 2011a). As a consequence, the actual transition to the autumn freeze-up was postponed until the end of the 4th period (Fig. 20a). While the height to the top of these clouds was variable in time, towards the end the cloud layer subsided and eventually dissipated around 31 August (DoY 244) at the end of the 4th period. The 5th and final period had a low-level cloud fraction below 300–400 m and no cloud at all above 1 km, and showed the real onset of the freeze. The surface energy budget became negative (Sedlar et al., 2011a) and the

**Central Arctic
atmospheric summer
conditions during
ASCOS**

M. Tjernström et al.

Title Page

Abstract

Introduction

Conclusions

References

Tables

Figures



Back

Close

Full Screen / Esc

Printer-friendly Version

Interactive Discussion



temperature rapidly dropped to -12°C , although there was a temporary recovery of the temperature due to reappearing low-level clouds midday on 1st September (DoY 245) (see remaining surface temperature in Fig. 20a, after the mast had been taken down). The ice-drift was terminated at midnight between 1 and 2 September (DoY 246.0) but available observations suggest that the surface remained frozen after this (not shown).

Determining the onset of the freeze depends on the definition used. Many studies of different types, using different instrumentation, show a general consensus that the Central Arctic freeze onset often occurs between the 2nd week of August and early September (e.g., Rigor et al., 2000; Belchansky et al., 2004; Overland et al., 2008). One definition is the first time that a running-mean near-surface air temperature falls below a somewhat arbitrary threshold, e.g. -2°C , to identify the freeze onset. In Fig. 20 the near-surface air temperature, low-pass filtered at a cutoff frequency of two weeks, is shown as the dashed red line. It passes below this threshold at DoY 236 (23 August) consistent with the picture that freeze onset was triggered by the cold 3rd period and solidified by the change in albedo by the snowfall associated with the weather system on DoY 236 (23 August). Note however that the exact timing of -2°C crossing is sensitive to the exact specifications in the low-pass filter design. The actual freeze started almost a week later, when the low-level clouds broke up, allowing the surface to cool rapidly in the longwave (Sedlar et al., 2011a). In essence this means that the end of the melt and the beginning of the freeze did not necessarily coincide. Regardless of the definition used and exact date of end-of-melt/freeze-up, it is clear that ASCOS succeeded in capturing this important transition for 2008 during the ice drift.

The thermodynamic vertical structure of the five periods is illustrated by statistics of the profiles of equivalent potential temperature, Θ_e , and relative humidity with respect to ice, RH_i , in Figs. 21 and 22; Figs. 23 and 24 show median profiles of wind speed, and the vertical gradients of Θ_e and scalar wind speed for the five periods, respectively. The first two periods were similar in thermodynamical structure, while slightly different in detail. There was a well-mixed layer at almost 100 % relative humidity during the 1st period, reaching to ~ 500 m, while in the 2nd period the well-mixed layer was shallower

**Central Arctic
atmospheric summer
conditions during
ASCOS**

M. Tjernström et al.

Title Page

Abstract

Introduction

Conclusions

References

Tables

Figures

⏪

⏩

◀

▶

Back

Close

Full Screen / Esc

Printer-friendly Version

Interactive Discussion

(to ~ 100 – 200 m) and the moist layer deeper (to ~ 1 km). The wind speeds during the 1st period (Fig. 23) were significantly larger than during any of the other periods, including the 2nd. The temperature gradient from the first period (Fig. 24a) shows a shallow layer of unstable stratification close to the surface, approximately 70 m deep, with a near-neutral but slightly stable layer up to 300–500 m. The wind-speed gradient during this period, although the largest during the ice drift, approaches zero at about ~ 300 m (Fig. 24b). Thus even during in the 1st period, which had the most unstable conditions close to the surface and the largest wind shear, the surface-based boundary-layer was limited to about 300 m. The well-mixed layer in the 1st period was topped by a stably stratified layer that extended from about 500 m, up to the capping inversion at about 1 km (Fig. 24a). The 2nd period was slightly more stably stratified close to the surface, near-neutral up to 200 m. Then it becomes gradually more stable up to ~ 1 km; above this the structure is similar to the 1st period.

The 3rd period, although signified by lower near-surface temperatures, was still well-mixed near the surface, but only in the lowest ~ 50 m. This layer was capped by a strong inversion extending to 400–500 m with free-tropospheric conditions aloft (Figs. 21c and 24a). The corresponding moist layer was ~ 200 m deep and the RH_i in this layer was $> 100\%$ (Fig. 22c) consistent with the formation of frozen drizzle in the low-level cloud layer and the accumulation of rime and frost on the surface. The wind speed was the lowest during the ice drift (Fig. 23) with an indication of a weak low-level wind-speed maximum around 100–200 m. Consistent with this jet-like feature the wind-speed gradient crossed zero around 150 m and was negative but small up to ~ 300 m (Fig. 24b).

The 4th period had a somewhat deeper and only slightly stable near-neutral layer in the lowest 100 m and then was more stable but still near-neutral in the 200–800 m layer with a capping inversion at ~ 1 km. A clear double structure is visible in both Θ_e and RH_i , with a secondary well-mixed layer ~ 800 – 1000 m (Figs. 21d and 22d). In this double-layer structure RH_i first increased with height in the lowest 200 m followed by a slight minimum and a secondary maximum in the upper layer, well above 100 %. The

**Central Arctic
atmospheric summer
conditions during
ASCOS**

M. Tjernström et al.

Title Page

Abstract

Introduction

Conclusions

References

Tables

Figures

⏪

⏩

◀

▶

Back

Close

Full Screen / Esc

Printer-friendly Version

Interactive Discussion



upper of these well-mixed structures was associated with the stratocumulus cloud layer that was present for most of the 4th period. The wind shear during this period was zero above 200 m (Fig. 24b).

The 5th and final period displays a strong surface-based inversion up to ~ 100 m, by far the most stably stratified boundary layer during the ice drift, and is capped by a secondary inversion starting at 300 m and transitioning to free tropospheric conditions above 800 m (Figs. 21e and 24b). The second stable layer 100–500 m was likely the remnants of the dissipating subsidence inversion in which the stratocumulus layer was previously residing. As the cloud dissipated, the buoyancy-generated turbulence from the cloud, forced by cloud-top cooling, has dissipated and the layer was becoming increasingly stably stratified. The wind speed in the lowest kilometer increased during the 5th period and is the second strongest during the ice drift (Fig. 23) although the winds aloft are weaker and comparable to periods 2 and 4. The wind shear first approaches zero at around 150 m with a 100 m shallow layer of negative shear on top (Fig. 24a).

The 4th period is of special interest with its persistent stratocumulus layer and the deep boundary layer with two distinct well-mixed layers in the thermodynamical structure. Since the upper well-mixed layer was thermodynamically separated from the near-surface atmosphere and the wind shear goes to zero well below the upper layer, this suggests that the cloud layer was intermittently decoupled from the surface. This indicates the presence of a three-layer structure: 1) A shallow surface-based boundary layer, about ~ 200 m deep on average, where turbulence was predominantly driven by wind-shear; 2) An upper layer associated with the clouds, where turbulence was generated by buoyant overturning driven by cloud-top longwave cooling; 3) In between these two layers there was a second layer with near-neutral characteristics. From previous observations (e.g., Tjernström, 2005), the inversion base statistics in Fig. 13 and the depth of the shear layer in Fig. 24b, it seems unlikely that surface-based turbulence would be able to mix such a deep layer as from the surface and up through the cloud layer. The shear-driven boundary layer is too shallow to sustain the deep well-mixed

**Central Arctic
atmospheric summer
conditions during
ASCOS**

M. Tjernström et al.

Title Page

Abstract

Introduction

Conclusions

References

Tables

Figures

⏪

⏩

◀

▶

Back

Close

Full Screen / Esc

Printer-friendly Version

Interactive Discussion



layer observed in the thermal structure in Fig. 21d. The somewhat lower RH_i in the layer between 200 and 500 m also suggests that this intermediate layer has a different character. This suggests that the surface-based boundary layer is too shallow on its own to connect the surface layer and the stratocumulus layer. The well-mixed upper cloud layer, on the other hand, is generated by cloud-induced turbulence, from cloud-top cooling. If sufficiently strong this mixing may penetrate downward to the top of the surface based mixed layer. The upper and lower layers may then connect and turbulence can couple the surface and clouds, and transport, for example, moisture or aerosols between these layers. The well-mixed structure imposed on the layer between the top of the lower layer and the cloud layer during such mixing episodes may remain long after the mixing itself has ceased, like in a residual layer.

6 Summary and conclusions

We have presented an analysis of meteorological conditions encountered during the Arctic Summer Cloud Ocean Study (ASCOS). ASCOS was deployed on the Swedish icebreaker *Oden* through most of August and into early September, 2008, as part of the International Polar Year. The science focus of ASCOS was on the formation and life-cycle of low-level clouds and their effect on the surface energy budget. To accomplish this goal, ASCOS encompassed several scientific disciplines: meteorology, aerosol physics and chemistry, atmospheric chemistry, physical oceanography and marine biology.

In order to understand and generalize many of the processes studied during ASCOS, an understanding of the meteorological processes at play are necessary, and one objective of this paper is to provide an overview of the meteorological conditions that were encountered during ASCOS as a whole, and in particular during the ice drift. Research-quality observations from the Central Arctic Ocean are sparse and often taken over short time periods; interpreting the results requires analysis of the generality of the observations. Thus a second objective of this paper is to compare the

Central Arctic atmospheric summer conditions during ASCOS

M. Tjernström et al.

Title Page

Abstract

Introduction

Conclusions

References

Tables

Figures

⏪

⏩

◀

▶

Back

Close

Full Screen / Esc

Printer-friendly Version

Interactive Discussion



meteorological conditions during ASCOS with those from previous similar field studies in the Central Arctic during the summer season: the AOE-96, SHEBA and AOE-2001 expeditions from the summers of 1996, 1998 and 2001, respectively. Instead of comparing details for identical time periods, which would severely restrict the amount of data available, we compare statistics of all data available from these expeditions within the 1 July through 1 September time frame.

The main features of the synoptic conditions are summarized below:

- The ASCOS summer was characterized by a high-pressure anomaly over the Canada Basin and a low-pressure anomaly over Northern Norway into the Kara Sea. The high-pressure anomaly had an almost barotropic vertical structure, and generated an anomalous anticyclonic large-scale flow over much of the Arctic Ocean.
- As a result, several low-pressure systems propagated westward around the North Pole and across the path of ASCOS in the North-Atlantic sector of the Arctic, especially during the first half of the expedition. This is the opposite to the common storm track.
- The Siberian continent and Greenland had higher than average temperatures at the surface; aloft these two warm centers joined across the Arctic Ocean in a band of higher than average temperatures.
- Conditions over the Siberian Shelf region were moister than average but the ASCOS region was close to climatology in terms of low-level moisture and precipitable water.
- The ASCOS ice camp region was under the influence of significant synoptic-scale activity for the first half of the expedition, up until around 20 August, after which a high-pressure situation dominated until the end of the campaign.
- Air mass origins for the synoptically active period were mostly from the Kara and Greenland Seas. During the high-pressure dominated period the air mass origin

**Central Arctic
atmospheric summer
conditions during
ASCOS**

M. Tjernström et al.

Title Page

Abstract

Introduction

Conclusions

References

Tables

Figures

⏪

⏩

◀

▶

Back

Close

Full Screen / Esc

Printer-friendly Version

Interactive Discussion



was first from the Greenland region and then gradually shifted over to the Canadian Archipelago and then across the Western Arctic Ocean.

In terms of both basic near-surface meteorology and the vertical structure, ASCOS was broadly similar to the previous expeditions analyzed but there were some notable differences in details:

- Near-surface temperature was observed mostly in the -2 to 0°C interval, with a tail of lower temperatures in the probability distribution, reaching around -10°C . The cold tail in the probability distributions is a result of brief, colder episodes that start appearing in August in all expeditions examined; these were absent earlier in the summer. Conditions were consistently very moist, with relative humidity rarely $< 90\%$ while near-surface winds were most often in the $2\text{--}6\text{ m s}^{-1}$ range and seldom $> 10\text{ m s}^{-1}$.
- Cloud fraction was high during all expeditions and was dominated by low-level clouds. The lowest cloud base was most often below 100 m in all four expeditions and the lowest clouds were usually $200\text{--}500\text{ m}$ thick, although SHEBA had deeper cloud more frequently.
- Visibility observations, available only from the three *Oden*-based expeditions, indicate frequent fog conditions. Visibility outside fog was usually high, most often $> 20\text{--}30\text{ km}$ even below very low-level clouds, indicating an absence of haze. Visibility of less than 1 km , the WMO criteria for fog, was most common in ASCOS, at $\sim 25\%$ of the time, while the other two expeditions had low visibility $10\text{--}15\%$ of the time.
- Incoming and net longwave surface radiation was mostly between $300\text{--}320$ and $-10\text{--}0\text{ W m}^{-2}$, respectively, in all four expeditions, with significant negative tails in the distributions coming from a few cloud free episodes. Solar radiation, incoming as well as net, was distinctly different for SHEBA. In the *Oden*-based expeditions, incoming and net solar radiation peaks at ~ 100 and $20\text{--}30\text{ W m}^{-2}$, respectively;

**Central Arctic
atmospheric summer
conditions during
ASCOS**

M. Tjernström et al.

Title Page

Abstract

Introduction

Conclusions

References

Tables

Figures



Back

Close

Full Screen / Esc

Printer-friendly Version

Interactive Discussion



**Central Arctic
atmospheric summer
conditions during
ASCOS**

M. Tjernström et al.

[Title Page](#)[Abstract](#)[Introduction](#)[Conclusions](#)[References](#)[Tables](#)[Figures](#)[Back](#)[Close](#)[Full Screen / Esc](#)[Printer-friendly Version](#)[Interactive Discussion](#)

in SHEBA the values were often higher, giving rise to a very broad and skewed probability distribution, although the broad peak is in the same range as for the three *Oden*-based expeditions. This could be caused by several factors that were different during SHEBA: a location farther south, a smaller cloud liquid water path and a lower surface albedo contribute to higher values of incoming and net solar radiation.

- Turbulent fluxes are in general small, within $\pm 10 \text{ W m}^{-2}$; however, as stated by Sedlar et al. (2011a) they are typically similar in size to the residual in the surface energy budget, i.e. the heat that remains available for freezing or melting, and are therefore still of importance.
- ASCOS, like the other three expeditions, featured a well-mixed and very moist boundary layer, capped by an inversion. The depth of the mixed layer and the height, depth and stability of the main capping inversion were different in the four expeditions, but the basic structure is very similar across all of them.
- Another common feature in all the expeditions was a very moist near-surface layer, which often reached well above the depth of the well-mixed layer. This indicates that specific moisture often increases above the capping inversion, unlike conditions in mid-latitude and sub-tropical boundary layers. This means that entrainment of air from the free troposphere can be a source of boundary-layer moisture and can act to maintain the high moisture near the surface. This is one aspect contributing to the very high boundary-layer relative humidity.
- The ASCOS ice drift spanned the end-of-melt/freeze onset transition. This transition is related to synoptic-scale meteorology; snowfall from synoptic systems and deposition of frost and rime increased the surface albedo at a time when net surface energy fluxes were approaching zero. This altered the surface energy budget sufficiently that surface melt conditions could not reestablish.

- The transition to colder temperatures after the end of the melt season was delayed almost a week by the presence of a persistent stratocumulus cloud layer that, by its surface radiative forcing, prevented the surface energy balance from becoming negative (Sedlar et al., 2011a). In a sense one can say that the start of the real freeze did not coincide with the end of the melt; there was an almost week-long period in between.

Taken together with previous expeditions a common picture emerges, with high amounts of low-level clouds in a well-mixed shallow boundary layer capped by a weak or moderately strong inversion, where high humidity, and sometimes also cloud top, penetrates well into the inversion. Turbulence in this system is generated at the surface and in the cloud layer. At the surface, turbulence generation is predominantly due to wind shear; although convective conditions occurred, the sensible heat flux was always small ($< 10 \text{ W m}^{-2}$). This layer is typically shallow, usually some 200 m deep, except during a few high-wind periods. In the cloud layer, turbulence is produced by buoyancy driven by cloud-top radiative cooling. This process is independent of the surface and the layered boundary-layer structure may be understood in terms of the relative importance of these two processes.

If the cloud layer is low enough, or the cloud-generated turbulence strong enough, the mixing may reach well below the cloud base and even into the surface based mixed layer. If, on the other hand, the clouds are sufficiently elevated or the cloud-induced turbulence is weaker, the layers will be separated. Sedlar et al. (2012) show that a redistribution of some cloud liquid water above the inversion base impact the longwave radiative cooling of the cloud layer, and thus alter the overturning buoyant motions driven by the cloud. The vertical structure encountered during ASCOS, especially during the 4th stratocumulus-dominated period of the ice drift may be a reflection of this, with its apparent three-layer structure, where the well-mixed middle layer may be a reflection of the sporadic coupling of the layers. This would explain the deep well-mixed structure, which is substantially deeper than the shear layer. Much of the boundary-layer mixing is therefore due to cloud-top cooling and subsequent buoyant overturning

Central Arctic atmospheric summer conditions during ASCOS

M. Tjernström et al.

Title Page

Abstract

Introduction

Conclusions

References

Tables

Figures

⏪

⏩

◀

▶

Back

Close

Full Screen / Esc

Printer-friendly Version

Interactive Discussion



of the cloud, implying a connection between the clouds and the free troposphere due to entrainment at the cloud top.

ACPD

12, 4101–4164, 2012

Central Arctic atmospheric summer conditions during ASCOS

M. Tjernström et al.

Title Page

Abstract

Introduction

Conclusions

References

Tables

Figures



Back

Close

Full Screen / Esc

Printer-friendly Version

Interactive Discussion



Acknowledgement. This work is part of the Arctic Summer Cloud-Ocean Study (ASCOS). ASCOS was an IPY project under the AICIA-IPY umbrella and an endorsed SOLAS project. ASCOS was made possible by funding from the Knut and Alice Wallenberg Foundation, the DAMOCLES Integrated Research Project from the European Union 6th Framework Program and the Swedish National Research Council (VR) while the Swedish Polar Research Secretariat provided access to the icebreaker *Oden* and logistical support. Support from the US National Science Foundation (NSF) and the National Atmospheric and Oceanic Administration for the remote sensing instruments for the cloud observations and from the UK Natural Environment Research Council (NERC) for some of the surface exchange and boundary-layer observations is gratefully acknowledged. MT, CL, TM & JS were also funded by VR, DAMOCLES and the Bert Bolin Center for Climate Research at Stockholm University, IMB and CEB were funded by the NERC while MDS POGP, CRW and MS were funded by the NSF. CEB was additionally funded by the UK Met Office, while JP was supported by the Academy of Finland, the Finnish Academy of Science and the Letters/Vilho, Yrjö and Kalle Väisälä Foundation. We are grateful to the science teams from AOE-96, SHEBA and AOE-2001 for supplying data. Finally we are indebted to the *Oden's* Captain Mattias Peterson and his crew for invaluable assistance with many things during the field deployment of ASCOS.

References

- ACIA: Impacts of a Warming Arctic: Arctic Climate Impact Assessment, Cambridge University Press, Cambridge, 2005.
- Belchansky, G. I., Douglas, D. C., and Platonov, N. G.: Duration of the Arctic sea ice melt season: regional and interannual variability, 1979–2001, *J. Clim.*, 17, 67–80, 2004.
- Birch, C. E., Brooks, I. M., Tjernström, M., Shupe, M. D., Mauritsen, T., Sedlar, J., Lock, A. P., Earnshaw, P., Persson, P. O. G., Milton, S. F., and Leck, C.: Modelling atmospheric structure, cloud and their response to CCN in the Central Arctic: ASCOS case studies, *Atmos. Chem. Phys. Discuss.*, 12, 2559–2601, doi:10.5194/acpd-12-2559-2012, 2012.
- Bromwich, D. H., Kuo, Y.-H., Serreze, M., Walsh, J., Bai, L.-S., Barlage, M., Hines, K. M., and Slater, A.: Arctic system reanalysis. Call for community involvement, *Eos, Trans. Amer. Geophys. Union*, 91, 13–14, 2010.

Central Arctic atmospheric summer conditions during ASCOS

M. Tjernström et al.

Title Page

Abstract

Introduction

Conclusions

References

Tables

Figures



Back

Close

Full Screen / Esc

Printer-friendly Version

Interactive Discussion



Central Arctic atmospheric summer conditions during ASCOS

M. Tjernström et al.

Title Page

Abstract

Introduction

Conclusions

References

Tables

Figures

⏪

⏩

◀

▶

Back

Close

Full Screen / Esc

Printer-friendly Version

Interactive Discussion

- Chapman, W. L. and Walsh, J. E.: Simulations of Arctic temperature and pressure by global coupled models. *J. Clim.*, 20, 609–632, doi:10.1175/JCLI4026.1, 2007.
- Curry, J. A. and Ebert, E. E.: Annual cycle of radiative fluxes over the Arctic Ocean: Sensitivity to cloud optical properties, *J. Clim.*, 5, 1267–1280, 1992.
- 5 Dee, D. P., Uppala, S. M., Simmons, A. J., Berrisford, P., Poli, P., Kobayashi, S., Andrae, U., Balmaseda, M. A., Balsamo, G., Bauer, P., Bechtold, P., Beljaars A. C. M., van de Berg, L., Bidlot, J., Bormann, N., Delsol, C., Dragani, R., Fuentes, M., Geer, A. J., Haimberger, L., Healy, S.B., Hersbach, H., Holm, E. V., Isaksen L., Kållberg, P., Köhler, M., Matricardi, M., McNally, A. P., Monge-Sanz, B. M., Morcrette, J.-J., Park, B.-K., Peubey, C., de Rosnay, P.,
10 Tavolato, C., Thepaut, J.-N., and Vitart, F.: The ERA-Interim reanalysis: configuration and performance of the data assimilation system, *Q. J. R. Meteorol. Soc.*, 137, 553–597, 2011.
- Devasthale, A., Sedlar, J., and Tjernström, M.: Characteristics of water-vapour inversions observed over the Arctic by Atmospheric Infrared Sounder (AIRS) and radiosondes, *Atmos. Chem. Phys.*, 11, 9813–9823, doi:10.5194/acp-11-9813-2011, 2011.
- 15 Gascard, J.-C., Festy, J., le Goff, H., Weber, M., Bruemmer, B., Offermann, M., Doble, M., Wadhams, P., Forsberg, R., Hanson, S., Skourup, H., Gerland, S., Nicolaus, M., Metaxian, J.-P., Grangeon, J., Haapala, J., Rinne, E., Haas, C., Heygster, G., Jakobson, E., Palo, T., Wilkinson, J., Kaleschke, L., Claffey, K., Elder, B., and Bottenheim, J.: Exploring Arctic transpolar drift during dramatic sea ice retreat. *Eos, Trans. Amer. Geophys. Union*, 89, 21–22, 2008.
- 20 Holland, M. M. and Bitz, C. M.: Polar amplification of climate change in coupled models, *Clim. Dynam.*, 21, 221–232, 2003.
- Intrieri, J. M., Shupe, M. D., Uttal, T., and McCarty, B. J.: An annual cycle of Arctic clouds characteristics observed by radar and lidar at SHEBA, *J. Geophys. Res.*, 107, 8039, doi:10.1029/2000JC000423, 2002.
- 25 IPCC: Climate Change 2007: The Physical Science Basis. Contribution of Working Group I to the Fourth Assessment Report of the Intergovernmental Panel on Climate Change, edited by: Solomon, S., Qin, D., Manning, M., Chen, Z., Marquis, M., Averyt, K. B., Tignor, M., and Miller, H. L., Cambridge University Press, Cambridge, UK and New York, NY, USA, 2007.
- Kahl, J. D., Serreze, M. C., Shiotani, S., Skony, S. M., and Schnell, R. C.: In situ meteorological sounding archives for arctic studies, *B. Am. Meteorol. Soc.*, 73, 1824–1830, 1992.
- 30 Kahl, J. D., Martinez, D. A., and Zaitseva, N. A.: Long-term variability in the low level inversion layer over the Arctic Ocean, *Int. J. Clim.*, 16, 1297–1313, 1996.
- Karlsson, J. and Svensson, G.: The simulation of Arctic clouds and their influence on the winter

Central Arctic atmospheric summer conditions during ASCOS

M. Tjernström et al.

Title Page

Abstract

Introduction

Conclusions

References

Tables

Figures

⏪

⏩

◀

▶

Back

Close

Full Screen / Esc

Printer-friendly Version

Interactive Discussion



surface temperature in present-day climate in the CMIP3 multi-model dataset, *Clim. Dynam.*, 36, 623–635, doi:10.1007/s00382-010-0758-6, 2010.

Kay, J. E. and Gettelman, A.: Cloud influence on and response to seasonal Arctic sea ice loss, *J. Geophys. Res.*, 114, D18204, doi:10.1029/2009JD011773, 2009.

5 Kay, J. E., L'Ecuyer, T., Gettelman, A., Stephens, G., and O'Dell, C.: The contribution of cloud and radiation anomalies to the 2007 Arctic sea ice extent minimum, *Geophys. Res. Lett.*, 35, L08503, doi:10.1029/2008GL033451, 2008.

Leck, C., Bigg, E. K., Covert, D. S., Heintzenberg, J., Maenhaut, W., Nilsson, E. D., and Wiedensohler, A.: Overview of the atmospheric research program during the International Ocean Expedition of 1991 (IAOE-1991) and its scientific results, *Tellus B*, 48, 136–155, 1996.

10 Leck, C., Nilsson, E. D., Bigg, E. K., and Bäcklin, L.: The atmospheric program of the Arctic Ocean Expedition 1996 (AOE-1996) – an overview of scientific objectives, experimental approaches and instruments, *J. Geophys. Res.*, 106, 32051–32067, 2001.

Leck, C., Tjernström, M., Matrai, P., and Swietlicki, E.: Microbes, clouds and climate: can marine microorganisms influence the melting of the Arctic pack ice?, *EOS Trans. Amer. Geophys. Union*, 85, 25–36, 2004.

Lindsay, R. W. and Zhang, J.: The thinning of Arctic sea ice 1988–2003: have we passed a tipping point?, *J. Clim.*, 18, 4879–4894, 2005.

Liu, Y., Key, J. R., and Wang, X.: The influence of changes in cloud cover on recent surface temperature trends in the Arctic, *J. Clim.*, 21, 705–715, 2008

20 Overland, J. E.: The case for global warming in the Arctic, in: *Influence of Climate Change on the Changing Arctic and Sub-Arctic Conditions*, edited by: Nihoul, J. C. J. and Kostianoy, A. G., Nato Science for Peace and Security Series – C: Environmental Security, Springer, The Netherlands, 2009.

25 Overland, J. E., Wang, M., and Salo, S.: The recent Arctic warm period. *Tellus*, doi:10.1111/j.1600-0870.2008.00327.x, 2008

Persson, P. O. G., Fairall, C. W., Andreas, E. L., Guest, P. S., and Perovich, D. K.: Measurements near the Atmospheric Surface Flux Group tower at SHEBA: Near-surface conditions and surface energy budget, *J. Geophys. Res.*, 107, 8045, doi:10.1029/2000JC000705, 2002.

30 Persson, P. O. G., Solomon, A., and Shupe, M. D.: Melt season transition scenarios over sea ice from non-SHEBA in-situ data, *J. Geophys. Res.*, in preparation, 2012.

Richter-Menge, J. and Jeffries, M.: The Arctic, in “State of the Climate in 2010”, *B. Am.*

Central Arctic atmospheric summer conditions during ASCOS

M. Tjernström et al.

[Title Page](#)
[Abstract](#)
[Introduction](#)
[Conclusions](#)
[References](#)
[Tables](#)
[Figures](#)




[Back](#)
[Close](#)
[Full Screen / Esc](#)
[Printer-friendly Version](#)
[Interactive Discussion](#)


Meteorol. Soc., 92(6), S143–S160, 2011.

Rigor, I. G., Colony, R. L., and Martin, S.: Variations in surface air temperature observations in the Arctic 1979–1997, *J. Clim.*, 13, 896–914, 2000.

Sedlar, J. and Tjernström, M.: Stratiform cloud–inversion characterization during the Arctic melt season, *Bound. Layer-Meteorol.*, 132, 455–474, doi:10.1007/s10546-009-9407-1, 2009.

Sedlar, J., Tjernström, M., Mauritsen, T., Shupe, M. D., Brooks, I. M., Persson, P. O. G., Birch, C. E., Leck, C., Sirevaag, A., and Nicolaus, M.: A transitioning Arctic surface energy budget: the impacts of solar zenith angle, surface albedo and cloud radiative forcing, *Clim. Dynam.*, 37, 1643–1660, doi:10.1007/s00382-010-0937-5, 2011a.

Sedlar, J., Shupe, M. D., and Tjernström, M.: On the relationship between thermodynamic structure and cloud top, and its climate significance in the Arctic, *J. Clim.*, to be published, doi:10.1175/JCLI-D-11-00186.1, 2011b.

Serreze, M. C. and Francis, J.: The Arctic amplification debate, *Clim. Change*, 76, 241–264, 2006.

Serreze, M. C., Kahl, J. D., and Schnell, R. C.: Low-level temperature inversions of the Eurasian Arctic and comparisons with Soviet drifting station data, *J. Clim.*, 5, 615–629, 1992.

Serreze, M. C., Holland, M. M., and Stroeve, J.: Perspectives on the Arctic's shrinking sea-ice cover, *Science*, 315, 1533–1536, doi:10.1126/science.1139426, 2007.

Shupe, M. D. and Intrieri, J. M.: Cloud radiative forcing of the Arctic surface: the influence of cloud properties, surface albedo, and solar zenith angle, *J. Clim.*, 17, 616–628, 2004.

Shupe, M. D., Uttal, T., and Matrosov, S. Y.: Arctic cloud microphysics retrievals from surface-based remote sensors at SHEBA, *J. Appl. Meteor.*, 44, 1544–1562, 2005.

Shupe, M. D., Walden, V. P., Eloranta, E., Uttal, T., Campbell, J. R., Starkweather, S. M., and Shiobara, M.: Clouds at Arctic atmospheric observatories, part I: occurrence and macrophysical properties, *J. Appl. Meteor. Clim.*, 50, 626–644, 2011.

Sirevaag, A., de la Rosa, S., Fer, I., Nicolaus, M., Tjernström, M., and McPhee, M. G.: Mixing, heat fluxes and heat content evolution of the Arctic Ocean mixed layer, *Ocean Sci.*, 7, 335–349, doi:10.5194/os-7-335-2011, 2011.

Solomon, A., Shupe, M. D., Persson, P. O. G., and Morrison, H.: Moisture and dynamical interactions maintaining decoupled Arctic mixed-phase stratocumulus in the presence of a humidity inversion, *Atmos. Chem. Phys.*, 11, 10127–10148, doi:10.5194/acp-11-10127-2011, 2011.

Sorteberg, A., Furevik, T., Drange, H., and Kvamstø, N. G.: Effects of simulated

Central Arctic atmospheric summer conditions during ASCOS

M. Tjernström et al.

Title Page

Abstract

Introduction

Conclusions

References

Tables

Figures

⏪

⏩

◀

▶

Back

Close

Full Screen / Esc

Printer-friendly Version

Interactive Discussion

natural variability on Arctic temperature projections, *Geophys. Res. Lett.*, 32, L18708, doi:10.1029/2005GL023404, 2005.

Tjernström, M.: The summer Arctic boundary layer during the Arctic Ocean Experiment 2001 (AOE-2001), *Bound.-Layer Meteorol.*, 117, 5–36, 2005.

5 Tjernström, M.: Is there a diurnal cycle in the summer cloud-capped Arctic boundary layer?, *J. Atmos. Sci.*, 64, 3970–3986, 2007.

Tjernström, M. and Graversen, R. G.: The vertical structure of the lower Arctic troposphere analysed from observations and ERA-40 reanalysis, *Q. J. R. Meteorol. Soc.*, 135, 431–433, 2009.

10 Tjernström, M., Leck, C., Persson, P. O. G., Jensen, M. L., Oncley, S. P., and Targino, A.: The summertime Arctic atmosphere: meteorological measurements during the Arctic Ocean Experiment (AOE-2001), *B. Am. Meteorol. Soc.*, 85, 1305–1321, 2004a.

Tjernström, M., Leck, C., Persson, P. O. G., Jensen, M. L., Oncley, S. P., and Targino, A.: Experimental equipment: an electronic supplement to “The summertime Arctic atmosphere: meteorological measurements during the Arctic Ocean Experiment (AOE-2001)”, *B. Am. Meteorol. Soc.*, 85, 1322–1322, 2004b.

Tjernström, M., Zagar, M., Svensson, G., Cassano, J. C., Pfeifer, S., Rinke, A., Wyser, K., Dethloff, K., Jones, C., Semmler, T., and Shaw, M.: Modelling the Arctic boundary layer: an evaluation of six ARCMIP regional-scale models using data from the SHEBA project, *Bound.-Layer Meteorol.*, 117, 337–381, 2005.

20 Tjernström, M., Sedlar, J., and Shupe, M. D.: How well do regional climate models reproduce radiation and clouds in the Arctic?, *J. Appl. Meteorol. Clim.*, 47, 2405–2422, 2008

Tjernström, M., Leck, C., Birch, C. E., Brooks, B., Brooks, I. M., Bäcklin, L., Chang, R., Granath, E., Graus, M., Heintzenberg, J., Held, A., Hind, A., de la Rosa Høhn, S., Johnston, P., Knulst, J., Westberg, M., de Leeuw, G., Di Liberto, L., Martin, M., Matrai, P., Mauritsen, T., Müller, M., Norris, S., Orellana, M., Orsini, D., Paatero, J., Persson, O., Gao, Q., Rauschenberg, C., Ristovski, Z., Sedlar, J., Shupe, M. D., Sierau, B., Sirevaag, A., Sjögren, S., Stetzer, O., Swietlicki, E., Szczodrak, M., Vaattovaara, P., Wahlberg, N., and Wheeler, C.: The Arctic Summer Cloud-Ocean Study (ASCOS): overview and experimental design. *Atmos. Chem. Phys.*, in preparation, 2012.

30 Uttal, T., Curry, J. A., McPhee, M. G., Perovich, D. K., Moritz, R. E., Maslanik, J. A., Guest, P. S., Stern, H. L., Moore, J. A., Turenne, R., Heiberg, A., Serreze, M. C., Wylie, D. P., Persson, P. O. G., Paulson, C. A., Halle, C., Morison, J. H., Wheeler, P. A., Makshtas, A.,

**Central Arctic
atmospheric summer
conditions during
ASCOS**

M. Tjernström et al.

[Title Page](#)

[Abstract](#) [Introduction](#)

[Conclusions](#) [References](#)

[Tables](#) [Figures](#)

[⏪](#) [⏩](#)

[◀](#) [▶](#)

[Back](#) [Close](#)

[Full Screen / Esc](#)

[Printer-friendly Version](#)

[Interactive Discussion](#)

Welch, H., Shupe, M. D., Intrieri, J. M., Stamnes, K., Lindsey, R. W., Pinkel, R., Pegau, W. S., Stanton, T. P., and Grenfeld, T. C.: Surface heat budget of the Arctic Ocean, *B. Amer. Meteorol. Soc.*, 83, 255–276, 2002.

5 Wang, X. and Key, J. R.: Arctic Surface, Cloud, and Radiation Properties Based on the AVHRR Polar Pathfinder Data Set. Part I: Spatial and Temporal Characteristics, *J. Clim.*, 18, 2558–2574, 2005.

Walsh, J., Kattsov, V., Chapman, W., Govorkova, V., and Pavlova, T.: Comparison of Arctic climate simulations by uncoupled and coupled global models, *J. Clim.*, 15, 1429–1446, 2002.

10 Westwater, E. R., Han, Y., Shupe, M. D., and Matrosov, S. Y.: Analysis of integrated cloud liquid and precipitable water vapor retrievals from microwave radiometers during SHEBA, *J. Geophys. Res.*, 106, 32019–32030, 2001.



Central Arctic atmospheric summer conditions during ASCOS

M. Tjernström et al.

Title Page

Abstract

Introduction

Conclusions

References

Tables

Figures

◀

▶

◀

▶

Back

Close

Full Screen / Esc

Printer-friendly Version

Interactive Discussion



Table 1. Brief overview of measurements used for the comparison between the different expeditions.

Variables	ASCOS	Expedition		
		AOE-2001	SHEBA	AOE-96
Near-surface temperature, humidity and wind speed	Weather station onboard and mast on the ice	Weather station onboard and mast on the ice	Mast on the ice	Weather station onboard
Vertical thermodynamic structure	Radiosoundings (145) ^a	Radiosoundings (118) ^a	Radiosoundings (125) ^a	Radiosoundings (44) ^a
Inversion statistics	Scanning microwave radiometer	Scanning microwave radiometer	Radiosoundings	N/A ^b
Clouds	Laser ceilometer and MMCR	Laser ceilometer and Sband radar	MMCR and DABUL lidar	Laser ceilometer
Precipitable water and cloud liquid and ice water paths	Microwave radiometer and MMCR	N/A	Microwave radiometer and MMCR	N/A
Visibility	Backscatter visibility sensor	Backscatter visibility sensor	N/A	Backscatter visibility sensor
Long- and short-wave radiation	Broadband pyranometers and pyrgeometers on board and on ice	Broadband pyranometers and pyrgeometers on board and on ice	Broadband pyranometers and pyrgeometers on the ice	Broadband pyranometer and pyrgeometer on board
Turbulent fluxes and surface layer stability	Turbulence and profile instruments on the ice	Turbulence and profile instruments on the ice	Turbulence and profile instruments on the ice	N/A ^b

^a Number of soundings.

^b Insufficient sample length.

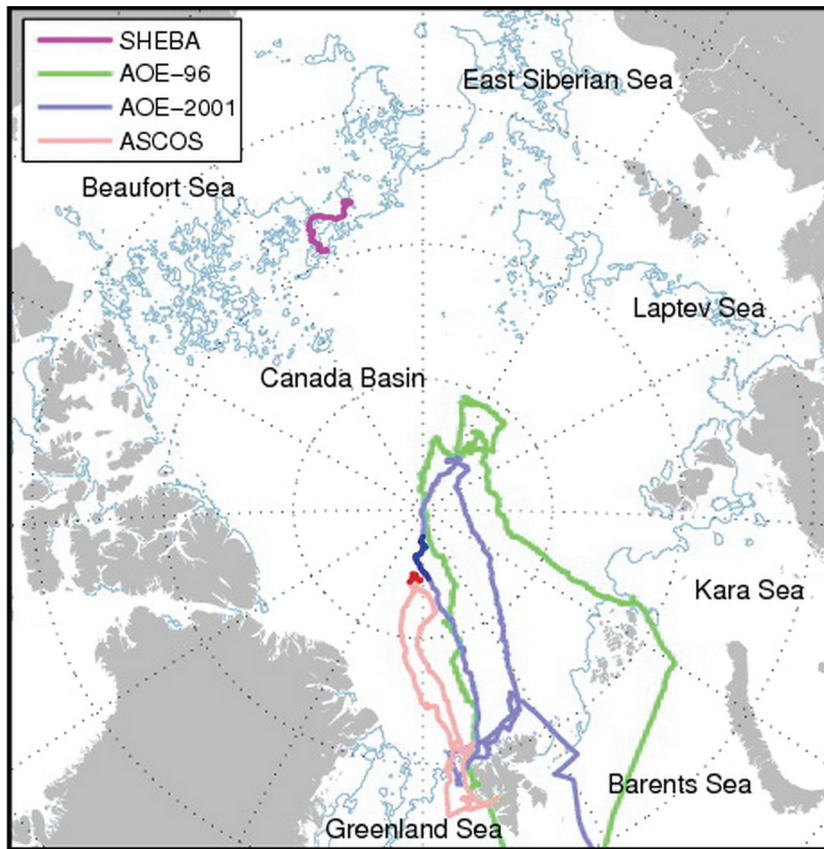


Fig. 1. Map with expedition tracks for ASCOS (red), the Arctic Ocean Experiment 2001 (AOE-2001; blue), the Arctic Ocean Experiment 1996 (AOE-96; green) and the Surface Heat Balance of the Arctic (SHEBA; magenta, July and August only). Ice drifts are marked by darker color and the thin blue line is the approximate 12 August ice boundary.

**Central Arctic
atmospheric summer
conditions during
ASCOS**

M. Tjernström et al.

Title Page

Abstract Introduction

Conclusions References

Tables Figures

◀ ▶

◀ ▶

Back Close

Full Screen / Esc

Printer-friendly Version

Interactive Discussion



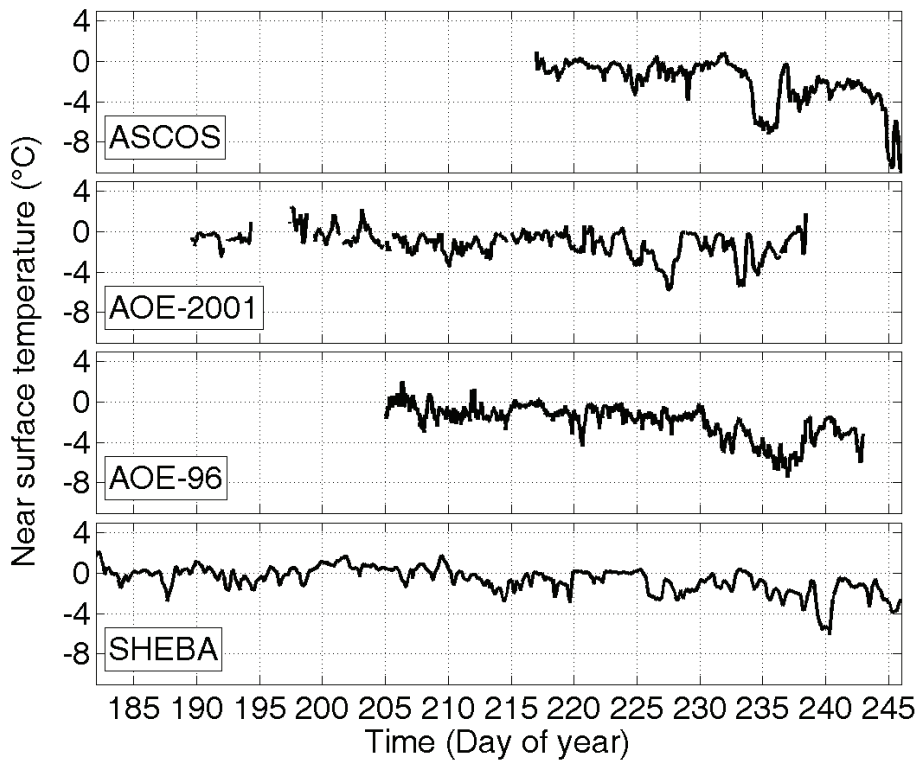


Fig. 2. Near surface temperature (°C) time series from the four expeditions, also illustrating the time periods used and the overlap in available data.

**Central Arctic
atmospheric summer
conditions during
ASCOS**

M. Tjernström et al.

Title Page

Abstract Introduction

Conclusions References

Tables Figures

◀ ▶

◀ ▶

Back Close

Full Screen / Esc

Printer-friendly Version

Interactive Discussion



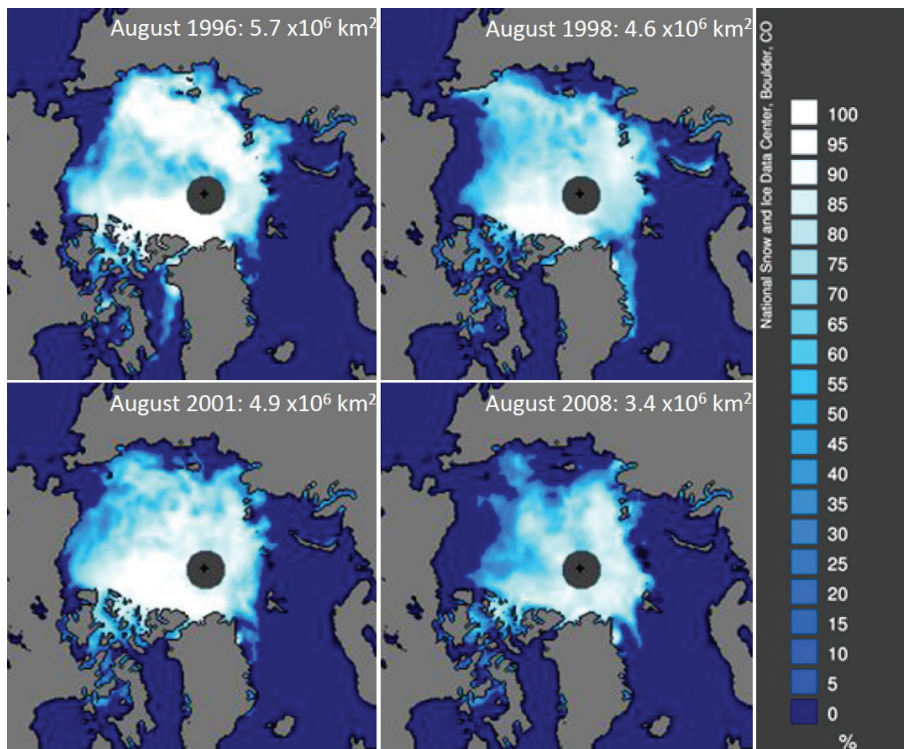


Fig. 3. Mean August sea-ice cover fraction for (a) 1996, (b) 1998, (c) 2001 and (d) 2008, from SSM/I satellite observations. The numbers in the top right of each panel indicate the total sea-ice area, excluding the area around the pole which is not covered by the satellite sensor. The data was obtained from the National Snow and Ice Data Center (NSIDC), Boulder, Colorado.

Central Arctic atmospheric summer conditions during ASCOS

M. Tjernström et al.

Title Page

Abstract Introduction

Conclusions References

Tables Figures

◀ ▶

◀ ▶

Back Close

Full Screen / Esc

Printer-friendly Version

Interactive Discussion



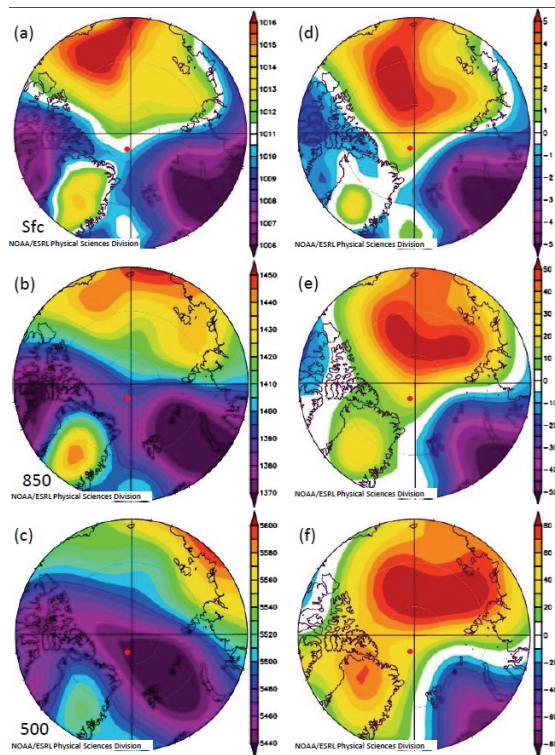


Fig. 4. Contour plots of the (a–c) mean and (d–f) anomaly to climate of mean sea-level pressure and 850 and 500 hPa geopotential height fields for the ASCOS period. The panels show (a, d) mean seal level pressure (hPa) and the (b, e) 850 hPa and (c, f) 500 hPa geopotential heights (m). Images are provided by the NOAA/ESRL Physical Sciences Division, Boulder Colorado from their Web site at <http://www.esrl.noaa.gov/psd/>, and uses the NCAR/NCEP reanalysis. Anomalies are calculated with respect to the period 1981–2010 mean. The approximate location of the ASCOS ice drift is marked by the red dot.

**Central Arctic
atmospheric summer
conditions during
ASCOS**

M. Tjernström et al.

Title Page

Abstract Introduction

Conclusions References

Tables Figures

⏪ ⏩

◀ ▶

Back Close

Full Screen / Esc

Printer-friendly Version

Interactive Discussion



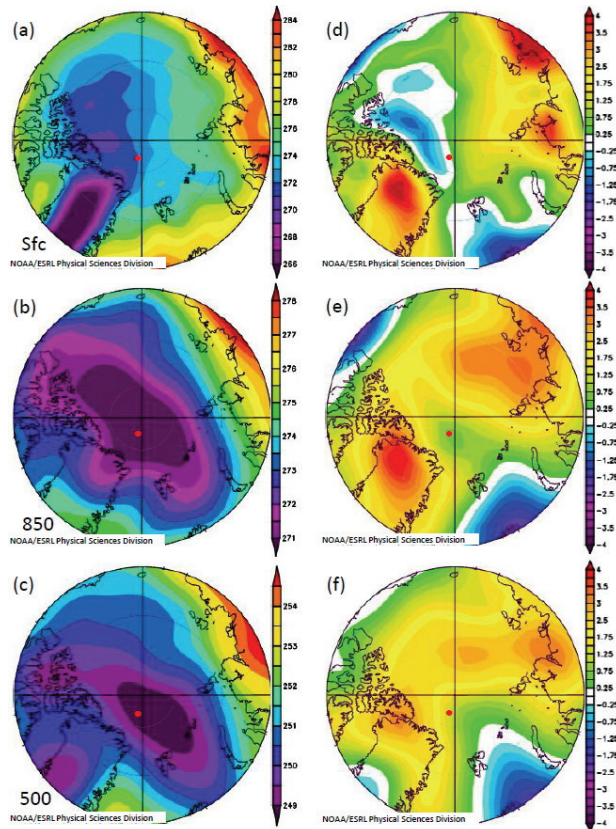


Fig. 5. Same as Fig. 4, but for temperature (K) **(a, d)** near the surface and at the **(b, e)** 850 and **(c, f)** 500 hPa pressure surfaces.

**Central Arctic
atmospheric summer
conditions during
ASCOS**

M. Tjernström et al.

Title Page

Abstract	Introduction
Conclusions	References
Tables	Figures

◀
▶

◀
▶

Back	Close
------	-------

Full Screen / Esc

Printer-friendly Version

Interactive Discussion



**Central Arctic
atmospheric summer
conditions during
ASCOS**

M. Tjernström et al.

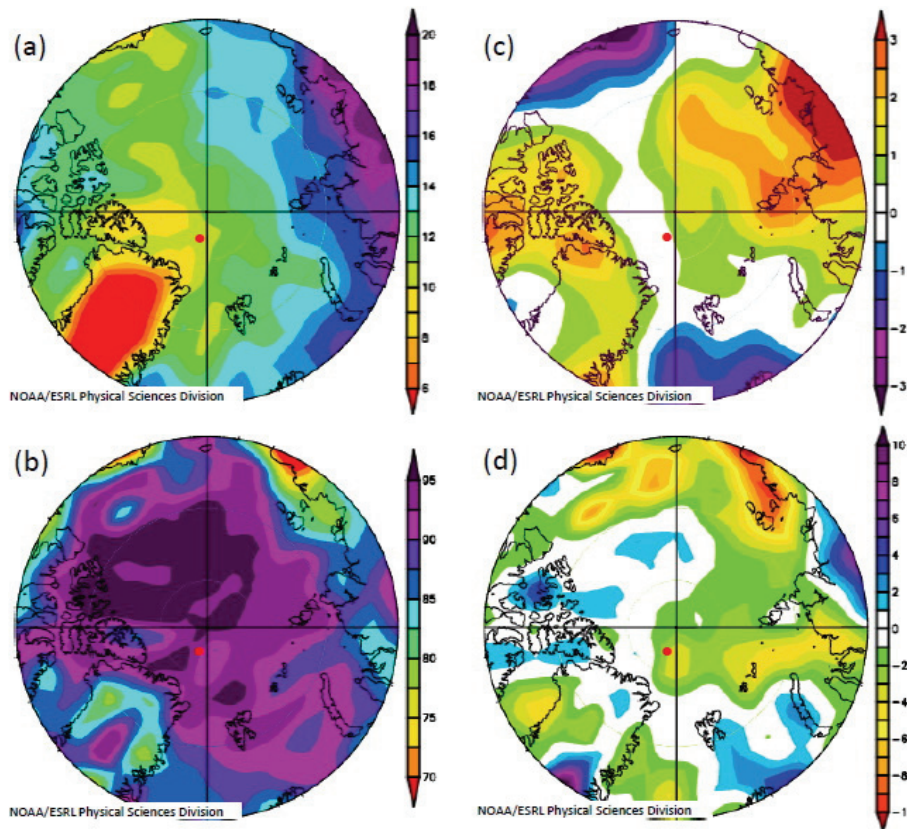


Fig. 6. Same as Fig. 4, but for **(a, c)** precipitable water (kg m^{-2}) and **(b, d)** near-surface relative humidity (%).

[Title Page](#)[Abstract](#)[Introduction](#)[Conclusions](#)[References](#)[Tables](#)[Figures](#)[◀](#)[▶](#)[◀](#)[▶](#)[Back](#)[Close](#)[Full Screen / Esc](#)[Printer-friendly Version](#)[Interactive Discussion](#)

Central Arctic atmospheric summer conditions during ASCOS

M. Tjernström et al.

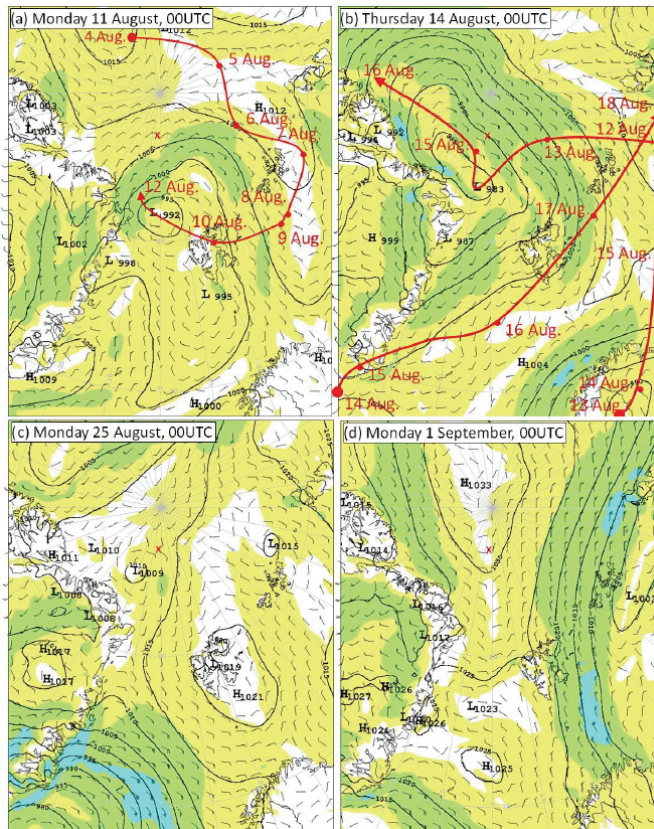


Fig. 7. Sea-level pressure and near-surface wind analyzes for four days during ASCOS: **(a)** 11, **(b)** 14, **(c)** 25 August and **(d)** 1 September 2008. Panels **(a)** and **(b)** also shows the storm tracks for the major low-pressure centers encountered early during ASCOS with location for the 00:00 UTC on days before and after the analyzes. The approximate location of the ASCOS ice drift is marked by the red x. See the text for a discussion.

[Title Page](#)
[Abstract](#)
[Introduction](#)
[Conclusions](#)
[References](#)
[Tables](#)
[Figures](#)
[⏪](#)
[⏩](#)
[◀](#)
[▶](#)
[Back](#)
[Close](#)
[Full Screen / Esc](#)
[Printer-friendly Version](#)
[Interactive Discussion](#)

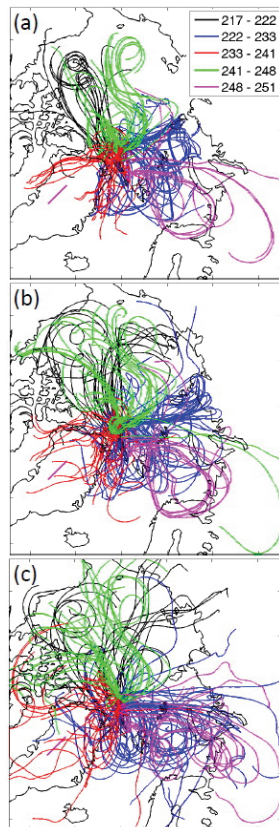


Fig. 8. Five-day back-trajectories calculated from the position of Oden at **(a)** 2 km, **(b)** 500 m and **(c)** 100 m receptor heights. The line colors indicate a rough sub-division into periods with different advection characteristics; see the text for a discussion.

Central Arctic atmospheric summer conditions during ASCOS

M. Tjernström et al.

Title Page	
Abstract	Introduction
Conclusions	References
Tables	Figures
◀	▶
◀	▶
Back	Close
Full Screen / Esc	
Printer-friendly Version	
Interactive Discussion	



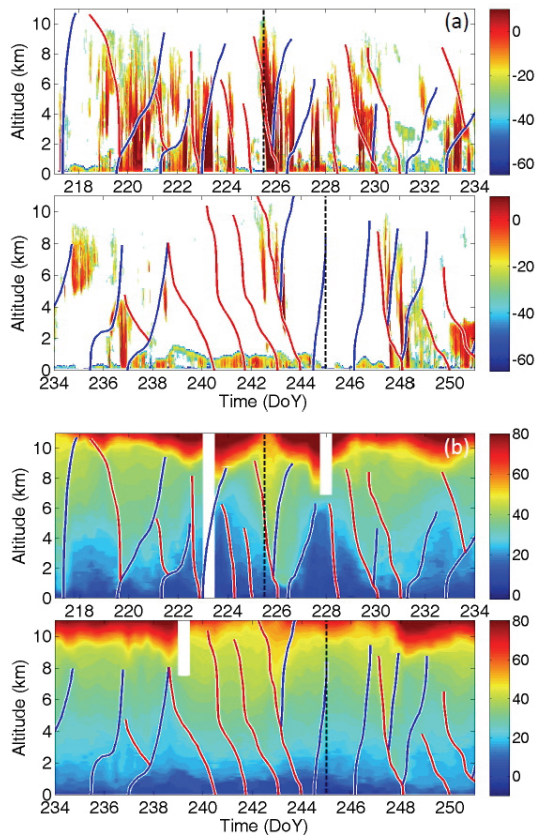


Fig. 9. Time-height cross section of **(a)** radar reflectivity (dBZ_e) from the MMCR cloud Doppler radar and **(b)** equivalent potential temperature (Θ_e , in $^{\circ}\text{C}$) from radiosoundings, also indicating subjectively analyzed (red) warm and (blue) cold frontal zones.

**Central Arctic
atmospheric summer
conditions during
ASCOS**

M. Tjernström et al.

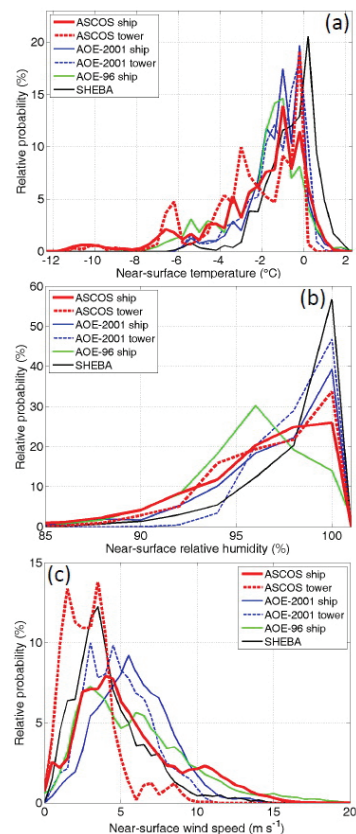


Fig. 10. Near-surface **(a)** temperature ($^{\circ}\text{C}$), **(b)** relative humidity (w.r.t. liquid, %) and **(c)** wind speed (m s^{-1}) from the ASCOS, AOE-2001, AOE-96 and SHEBA expeditions.

[Title Page](#)[Abstract](#)[Introduction](#)[Conclusions](#)[References](#)[Tables](#)[Figures](#)[◀](#)[▶](#)[◀](#)[▶](#)[Back](#)[Close](#)[Full Screen / Esc](#)[Printer-friendly Version](#)[Interactive Discussion](#)

**Central Arctic
atmospheric summer
conditions during
ASCOS**

M. Tjernström et al.

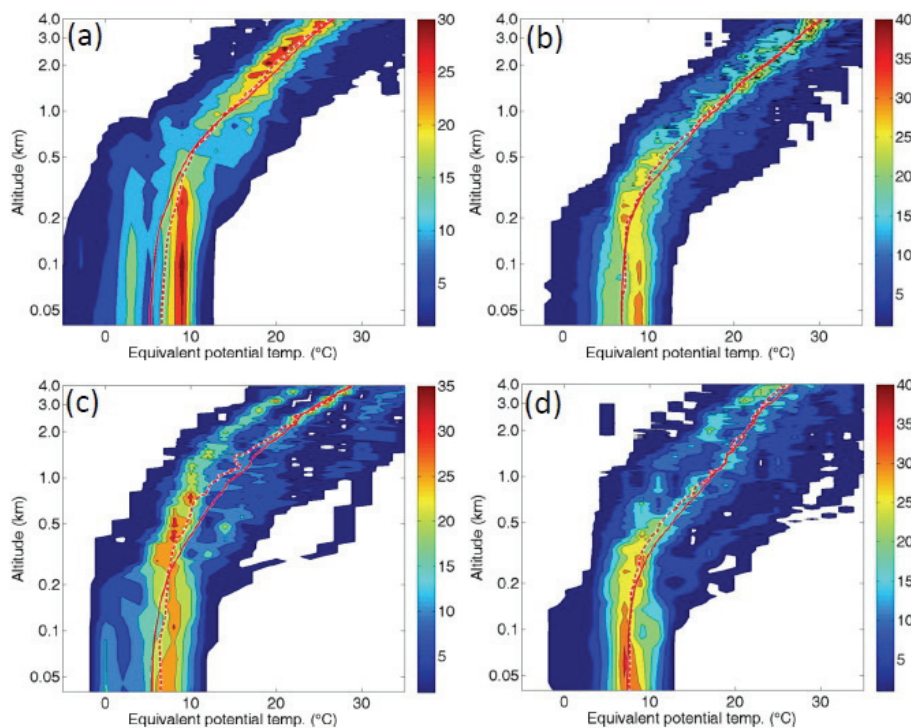


Fig. 11. Probability of equivalent potential temperature (Θ_e , in $^{\circ}\text{C}$) as a function of altitude (km) from (a) ASCOS, (b) AOE-2001, (c) AOE-96 and (d) SHEBA radiosoundings. Solid and dashed red lines are the mean and median profiles, respectively.

[Title Page](#)[Abstract](#)[Introduction](#)[Conclusions](#)[References](#)[Tables](#)[Figures](#)[◀](#)[▶](#)[◀](#)[▶](#)[Back](#)[Close](#)[Full Screen / Esc](#)[Printer-friendly Version](#)[Interactive Discussion](#)

**Central Arctic
atmospheric summer
conditions during
ASCOS**

M. Tjernström et al.

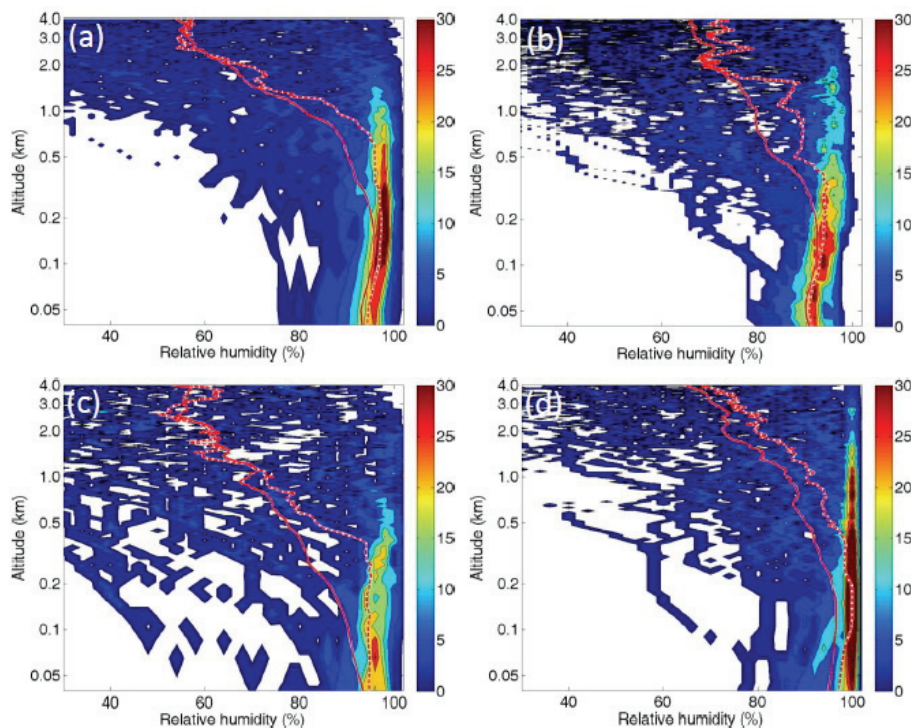


Fig. 12. Same as Fig. 11, but for relative humidity (%).

[Title Page](#)[Abstract](#)[Introduction](#)[Conclusions](#)[References](#)[Tables](#)[Figures](#)[◀](#)[▶](#)[◀](#)[▶](#)[Back](#)[Close](#)[Full Screen / Esc](#)[Printer-friendly Version](#)[Interactive Discussion](#)

Central Arctic atmospheric summer conditions during ASCOS

M. Tjernström et al.

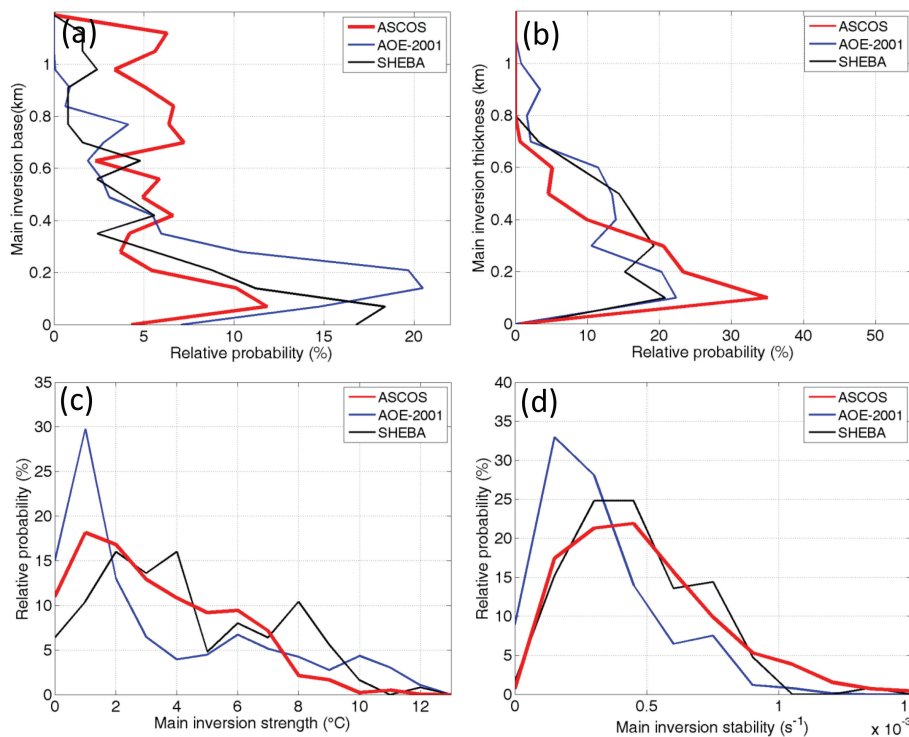


Fig. 13. Inversion statistics showing (a) the height to the base and (b) the thickness (km), and (c) strength ($^{\circ}\text{C}$) and (d) stability (Brunt Viasalla frequency, s^{-1}) of the main inversion from the (red) ASCOS, (blue) AOE-2001 and (black) SHEBA experiments. See the text for definitions and discussion.

Title Page

Abstract

Introduction

Conclusions

References

Tables

Figures

◀

▶

◀

▶

Back

Close

Full Screen / Esc

Printer-friendly Version

Interactive Discussion

**Central Arctic
atmospheric summer
conditions during
ASCOS**M. Tjernström et al.

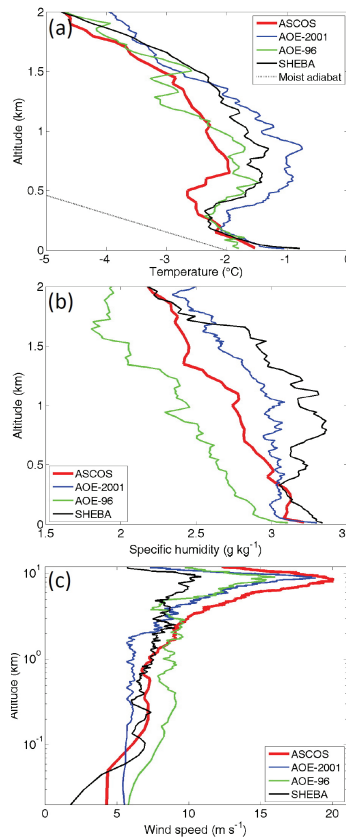
[Title Page](#)[Abstract](#)[Introduction](#)[Conclusions](#)[References](#)[Tables](#)[Figures](#)[◀](#)[▶](#)[◀](#)[▶](#)[Back](#)[Close](#)[Full Screen / Esc](#)[Printer-friendly Version](#)[Interactive Discussion](#)

Fig. 14. Median profiles of **(a)** temperature ($^{\circ}\text{C}$), **(b)** specific humidity (g kg^{-1}) and **(c)** wind speed (m s^{-1}) from the ASCOS, AOE-2001, AOE-96 and SHEBA radiosoundings. Note the logarithmic height scale in **(c)**.

Central Arctic atmospheric summer conditions during ASCOS

M. Tjernström et al.

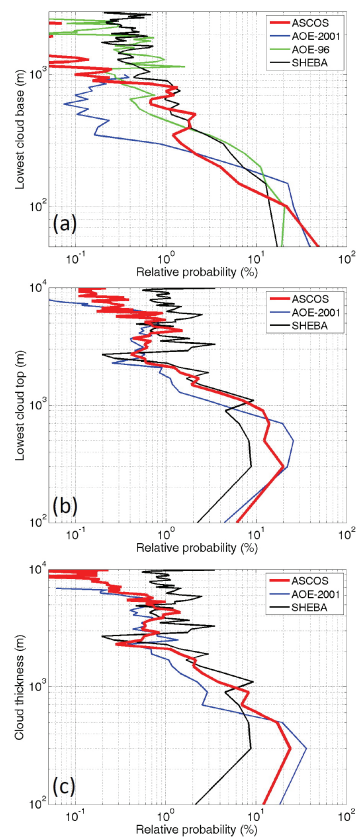


Fig. 15. Probability of **(a)** lowest cloud base, **(b)** lowest cloud top and **(c)** cloud thickness in meters from the ASCOS, AOE-2001, AOE-96 and SHEBA expeditions. Cloud base is estimated from laser ceilometers, while cloud top and thickness is additionally estimated using cloud-radar reflectivity (not available from AOE-96).

[Title Page](#)
[Abstract](#)
[Introduction](#)
[Conclusions](#)
[References](#)
[Tables](#)
[Figures](#)
[◀](#)
[▶](#)
[◀](#)
[▶](#)
[Back](#)
[Close](#)
[Full Screen / Esc](#)
[Printer-friendly Version](#)
[Interactive Discussion](#)

**Central Arctic
atmospheric summer
conditions during
ASCOS**

M. Tjernström et al.

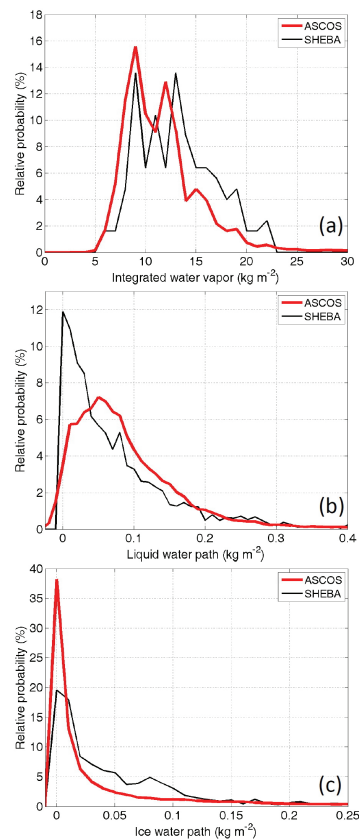


Fig. 16. Probability of total column integrated **(a)**, water vapor, **(b)** liquid water and **(c)** ice water paths (kg m^{-2}) from the ASCOS and SHEBA expeditions.

[Title Page](#)[Abstract](#)[Introduction](#)[Conclusions](#)[References](#)[Tables](#)[Figures](#)[◀](#)[▶](#)[◀](#)[▶](#)[Back](#)[Close](#)[Full Screen / Esc](#)[Printer-friendly Version](#)[Interactive Discussion](#)

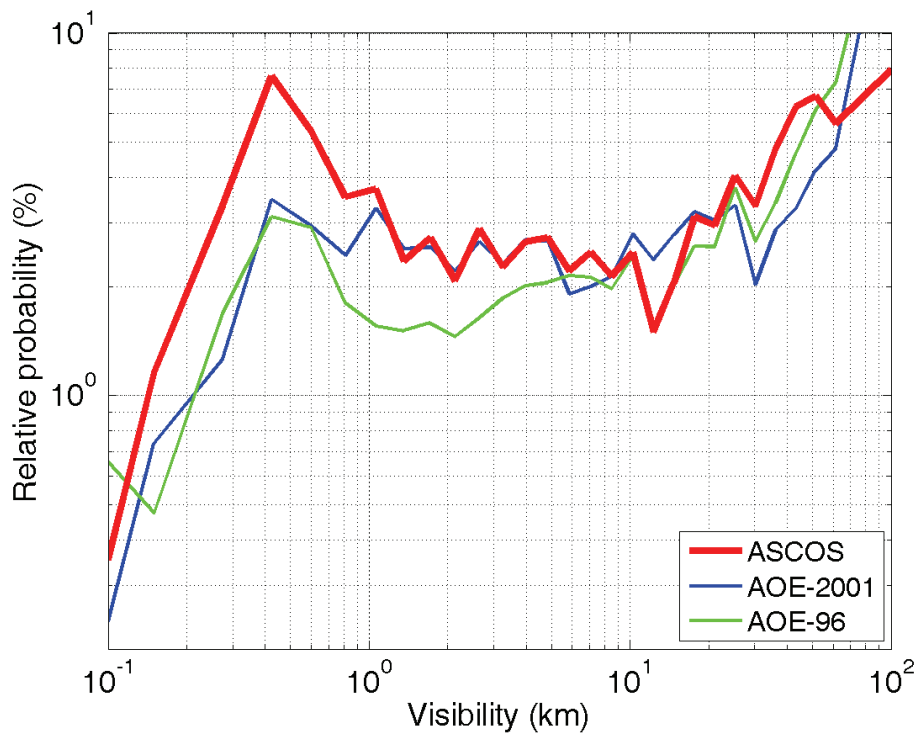


Fig. 17. Probability of visibility (km) from the ASCOS, AOE-2001 and AOE-96, estimated from a backscatter instrument.

**Central Arctic
atmospheric summer
conditions during
ASCOS**

M. Tjernström et al.

Title Page

Abstract	Introduction
Conclusions	References
Tables	Figures

◀	▶
◀	▶
Back	Close

Full Screen / Esc

Printer-friendly Version

Interactive Discussion



Central Arctic atmospheric summer conditions during ASCOS

M. Tjernström et al.

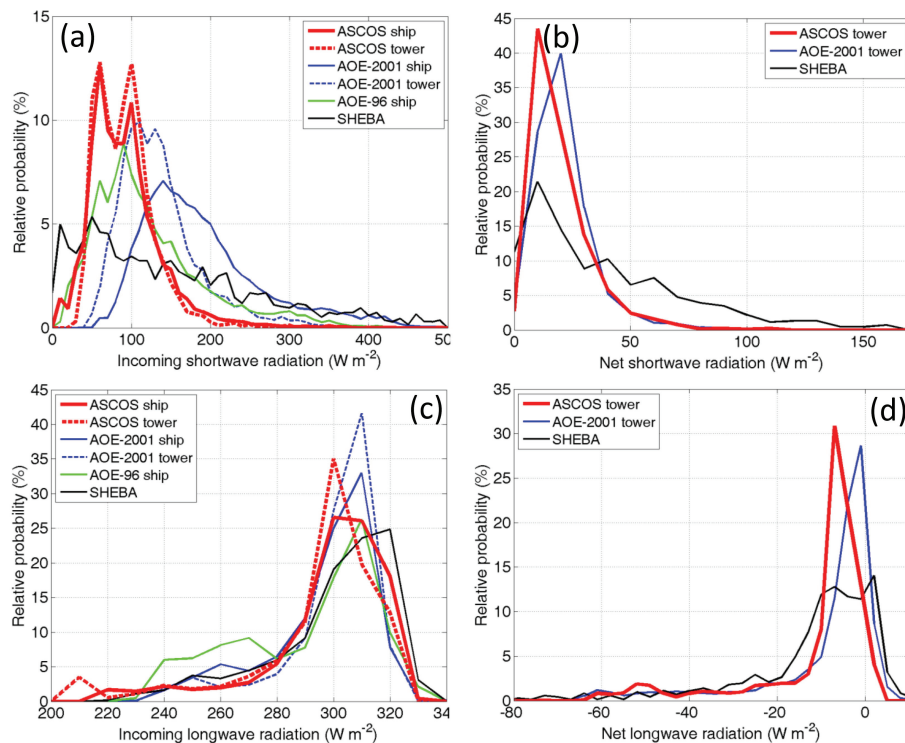


Fig. 18. Probability of (a, c) incoming and (b, d) net (a, b) shortwave and (c, d) longwave radiation in $W m^{-2}$ from the ASCOS, AOE-2001, AOE-96 and SHEBA expeditions. For ASCOS and AOE-2001 outgoing radiation is only available from the ice-drifts, when instruments were located on the ice, while from AOE-96 net radiation statistics could not be estimated due to the very short ice drift.

Title Page

Abstract

Introduction

Conclusions

References

Tables

Figures

◀

▶

◀

▶

Back

Close

Full Screen / Esc

Printer-friendly Version

Interactive Discussion

**Central Arctic
atmospheric summer
conditions during
ASCOS**

M. Tjernström et al.

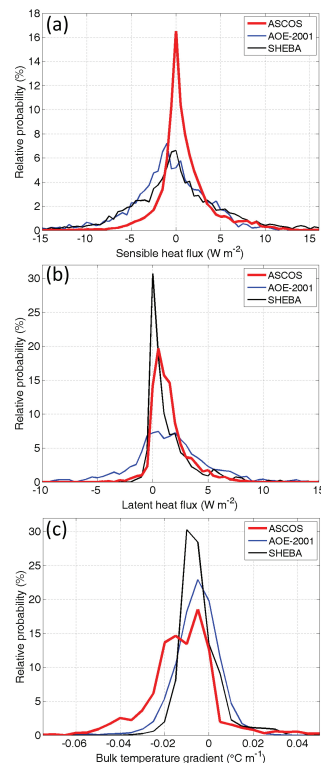


Fig. 19. Probability of **(a)** sensible and **(b)** latent heat flux (W m^{-2}), and **(c)** bulk near-surface temperature gradient ($^{\circ}\text{C m}^{-1}$) from the ASCOS, AOE-2001 and SHEBA expeditions. Turbulent fluxes are calculated from all eddy-correlation measurements within the surface layer ($< 15\text{ m}$) at each site and defined positive upward. The bulk temperature gradient is calculated as the temperature difference across the mast divided by the vertical distance between the sensors; temperature sensors were located at different heights in the different experiments but in all cases the difference is taken over roughly 8–10 m below a height of 15 m.

[Title Page](#)[Abstract](#)[Introduction](#)[Conclusions](#)[References](#)[Tables](#)[Figures](#)[◀](#)[▶](#)[◀](#)[▶](#)[Back](#)[Close](#)[Full Screen / Esc](#)[Printer-friendly Version](#)[Interactive Discussion](#)

Central Arctic atmospheric summer conditions during ASCOS

M. Tjernström et al.

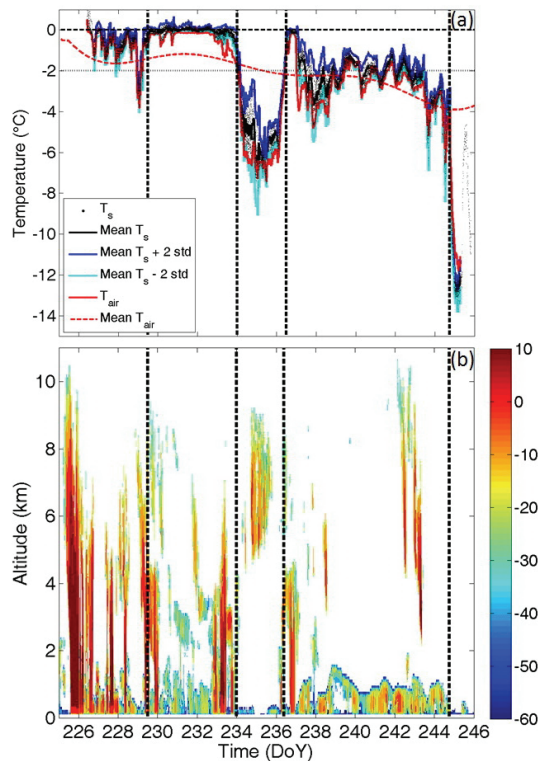


Fig. 20. In (a), time series of 12 individual surface temperature observations (black dots), their mean (solid black), the mean plus and minus two standard deviations, respectively (solid blue and cyan), measured (red) and low-pass filtered (red dashed) near surface air temperature, all in $^{\circ}\text{C}$. In (b), Time-height cross-section of radar reflectivity (dBZ_e) for the ice drift taken from the MMCR cloud radar. Vertical dashed lines show demarcation between the regimes discussed in the text.

Central Arctic atmospheric summer conditions during ASCOS

M. Tjernström et al.

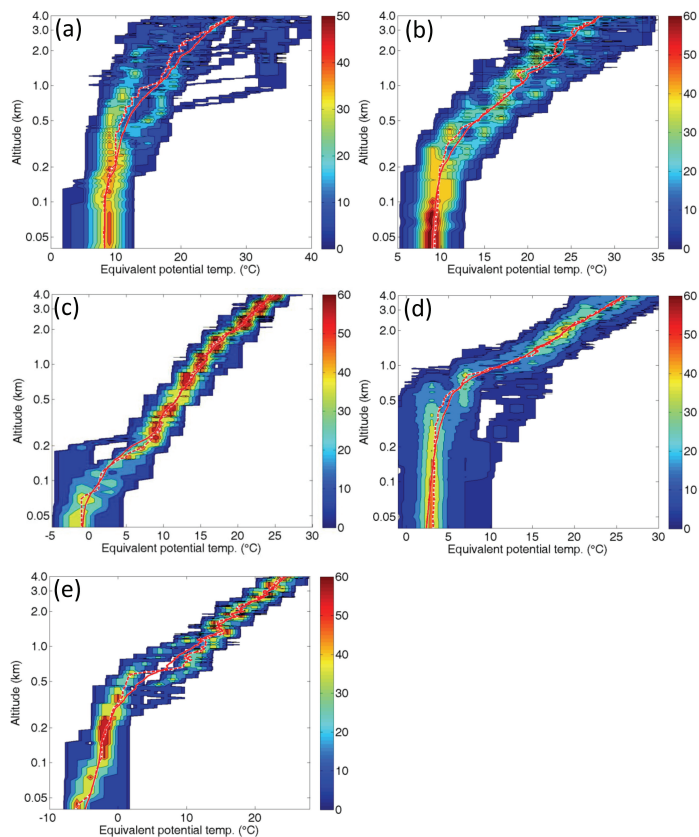


Fig. 21. Same as in Fig. 11 but for the five different periods defined in Fig. 20: **(a)** 1st, **(b)** 2nd, **(c)** 3rd, **(d)** 4th, **(e)** 5th periods.

[Title Page](#)[Abstract](#)[Introduction](#)[Conclusions](#)[References](#)[Tables](#)[Figures](#)[◀](#)[▶](#)[◀](#)[▶](#)[Back](#)[Close](#)[Full Screen / Esc](#)[Printer-friendly Version](#)[Interactive Discussion](#)

**Central Arctic
atmospheric summer
conditions during
ASCOS**

M. Tjernström et al.

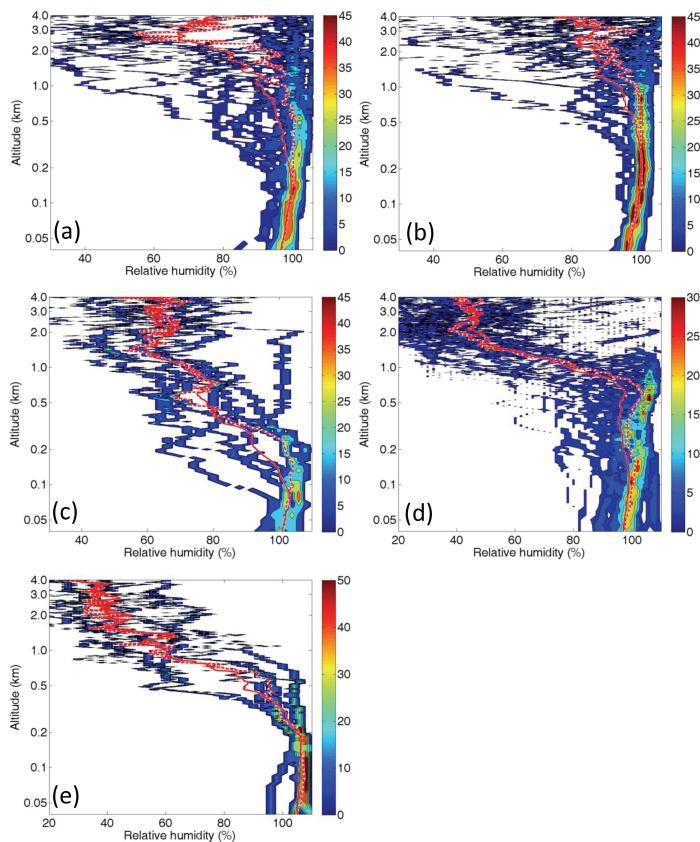


Fig. 22. Same as Fig. 21 but for relative humidity with respect to ice (%).

[Title Page](#)[Abstract](#)[Introduction](#)[Conclusions](#)[References](#)[Tables](#)[Figures](#)[◀](#)[▶](#)[◀](#)[▶](#)[Back](#)[Close](#)[Full Screen / Esc](#)[Printer-friendly Version](#)[Interactive Discussion](#)

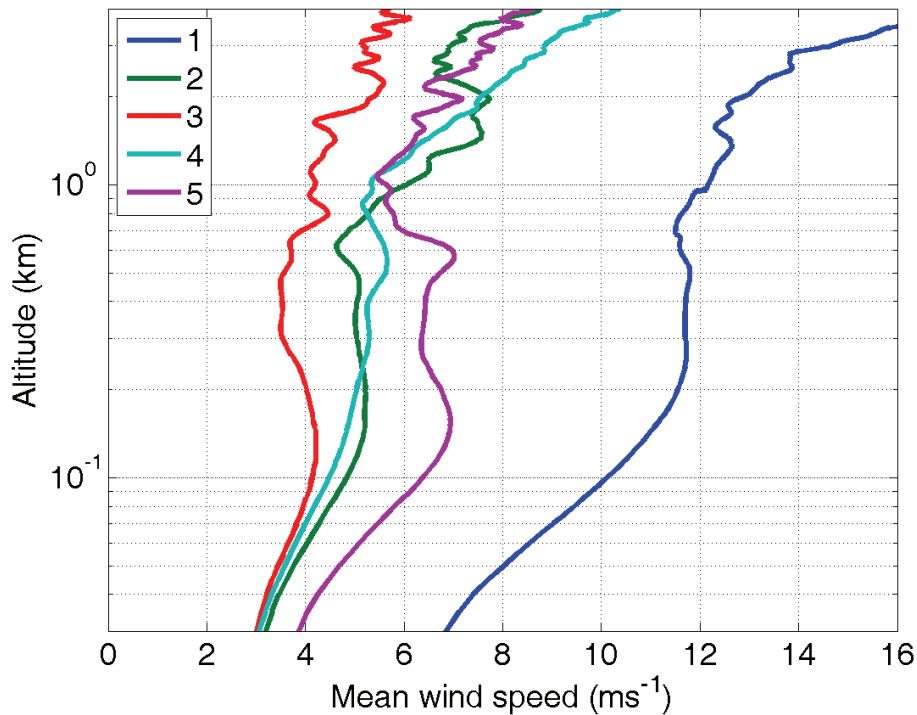


Fig. 23. Median wind-speed profiles (m s^{-1}) for the lowest 4 km, for the five periods defined in Fig. 20 and discussed in the text.

**Central Arctic
atmospheric summer
conditions during
ASCOS**

M. Tjernström et al.

Title Page

Abstract Introduction

Conclusions References

Tables Figures

◀ ▶

◀ ▶

Back Close

Full Screen / Esc

Printer-friendly Version

Interactive Discussion



Central Arctic
atmospheric summer
conditions during
ASCOS

M. Tjernström et al.

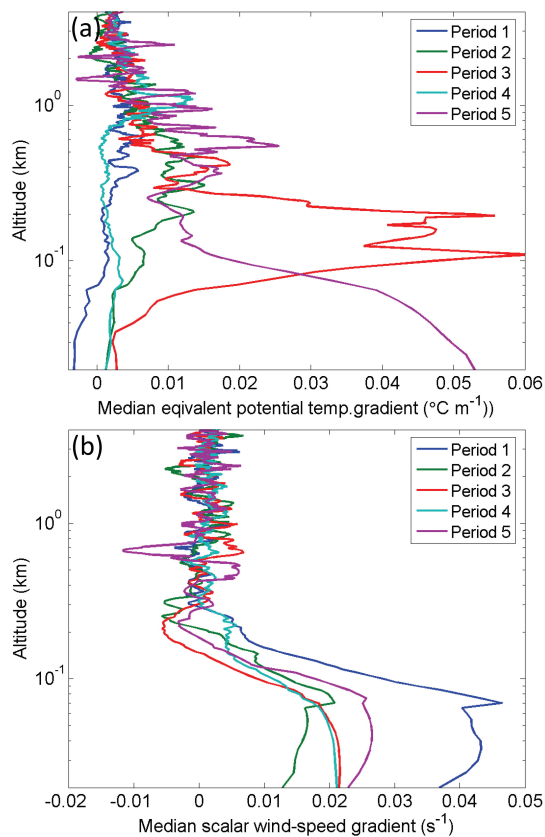


Fig. 24. Same as Fig. 23 but for the vertical gradients of **(a)** equivalent potential temperature (Θ_e , K m^{-1}) and **(b)** wind speed (s^{-1}).

[Title Page](#)[Abstract](#)[Introduction](#)[Conclusions](#)[References](#)[Tables](#)[Figures](#)[◀](#)[▶](#)[◀](#)[▶](#)[Back](#)[Close](#)[Full Screen / Esc](#)[Printer-friendly Version](#)[Interactive Discussion](#)